NASA Contractor Report 3337
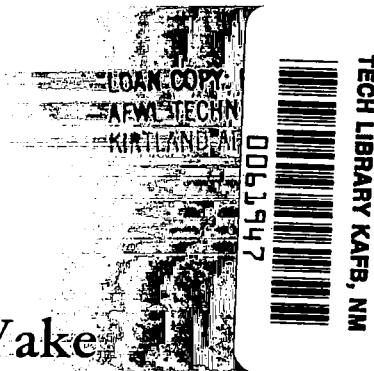
# Effect of Lateral Spacing on Wake Characteristics of Buildings

Earl Logan, Jr., and David S. Barber

NASA

NASA Contractor Report 3337

# Effect of Lateral Spacing on Wake Characteristics of Buildings

Earl Logan, Jr., and David S. Barber
*Arizona State University*
*Tempe, Arizona*

# NASA

National Aeronautics
and Space Administration

Scientific and Technical
Information Branch

1980

## FOREWORD

This study was initiated to determine wake profiles behind buildings and natural obstacles using a scaled model in a wind tunnel. The wind tunnel approach is preferable because of economy of time and money, simplicity and convenience. This is the third report of a continuing program sponsored by the Fluid Dynamics Branch, Atmospheric Sciences Division of the Space Sciences Laboratory at the George C. Marshall Space Flight Center, National Aeronautics and Space Administration, Huntsville, Alabama.

This research was conducted under the technical direction of Mr. Dennis W. Camp and Mrs. Margaret Alexander of the Space Sciences Laboratory at Marshall Space Flight Center. The support for this research was provided by Mr. John Enders, Solomon Weiss and A. Richard Tobiason of the Office of Aeronautics and Space Technology, NASA Headquarters, Washington, D.C.

# TABLE OF CONTENTS

# LIST OF TABLES

# LIST OF FIGURES

LIST OF FIGURES (Continued)

# NOMENCLATURE

A          Constant

$C_f$       Friction coefficient

$C_p$       Pressure coefficient

G          Equilibrium shape factor

H          Height of roughness element

U          Longitudinal mean velocity

$U_1$       Free stream mean velocity

$U*$        Friction velocity

UV         Component of Reynolds shear stress

U'         RMS value of longitudinal turbulence intensity

V          Vertical mean velocity

V'         RMS value of vertical turbulence intensity

W          Lateral mean velocity

W'         RMS value of lateral turbulence intensity

X          Longitudinal coordinate

Y          Distance from floor and wind tunnel

Z          Lateral coordinate

## Greek Alphabet

$\delta$          Boundary layer thickness

$\Delta$          "Clauser" thickness

$\kappa$          Von Karman constant

$\nu$          Kinematic viscosity

$\theta$          Momentum thickness

# CHAPTER 1

## INTRODUCTION

Sources of hazardous low-level wind conditions around airports have been discussed by Fichtl, Camp and Frost (1977). Wakes from bluff bodies, such as buildings, are among the sources mentioned. This is especially true of STOL vehicles landing or taking off over buildings, fences or other obstacles. Research which can predict the extent and severity of wind speed change is currently needed.

Experimental work undertaken at NASA Marshall Space Flight Center has been reported by Frost and Shahabi (1977) and by Frost, et al. (1977). This work involved the use of instrumented wind towers to study the wake of a simulated block building 3.2 m high by 26.8 m long under field conditions. Mean horizontal and turbulence profiles were determined from readings of anemometers located at heights z of 3, 6.2, 12 and 20.88 m above the ground.

The velocity and turbulence profiles measured in the field have been compared with wind tunnel profiles in the wake of a 1/50-scale model of the 3.2 x 2.4 x 26.8 m building. The results of the model study were reported by Woo, Peterka and Cermak (1977), and a comparison of data was presented by Logan and Camp (1978).

Logan and Camp (1978) found that field measurements of velocity and turbulence in the wake of the block building 3.2m high and 26.8m long show an apparent increase in momentum flow above the upwind value. The effect

has been studied by Logan and Chang (1980) in a pipe flow apparatus in which a fully developed boundary layer is disturbed by a single roughness element or obstacle. A second element, simulating the building, is placed at various downstream distances from the first obstacle; and velocity and turbulence profiles, measured by constant temperature hot-wire anemometer, are presented for regions upstream and downstream of the simulated building. Velocity-deficit and turbulence-excess decay characteristics of the disturbed or nonequilibrium layer are correlated with power law exponents and apparent roughness length at various distances downstream of the disturbance. Model wake profiles from the simulated building wake profiles to upstream nonequilibrium parameters are presented.

It is evident from the studies cited above that obstacles affect the wakes that occur immediately behind the obstacles. It is to be expected that wakes spread laterally as well, so that regions of the atmosphere near but not directly behind the obstacles are affected. This suggests a three-dimensional wake of some complexity near the ends of buildings aligned transverse to the wind.

The presence of adjacent buildings should complicate the flow further. If the buildings are near enough, the wakes formed near the ends should merge to form a resultant wake at some point downstream of the gap between them. In addition, small gaps between buildings would be expected to result in an acceleration of the surface flow.

To model end effects and gap effects in a single experiment, two bars of square cross section were mounted on the floor of a wind tunnel, as shown in Fig. 1. The spacing between the ends of the models was varied widely,

Flow direction

Adjusting screw

Building models

Plan View

3

Side of wind tunnel

Building models

Floor of wind tunnel

Sectional View
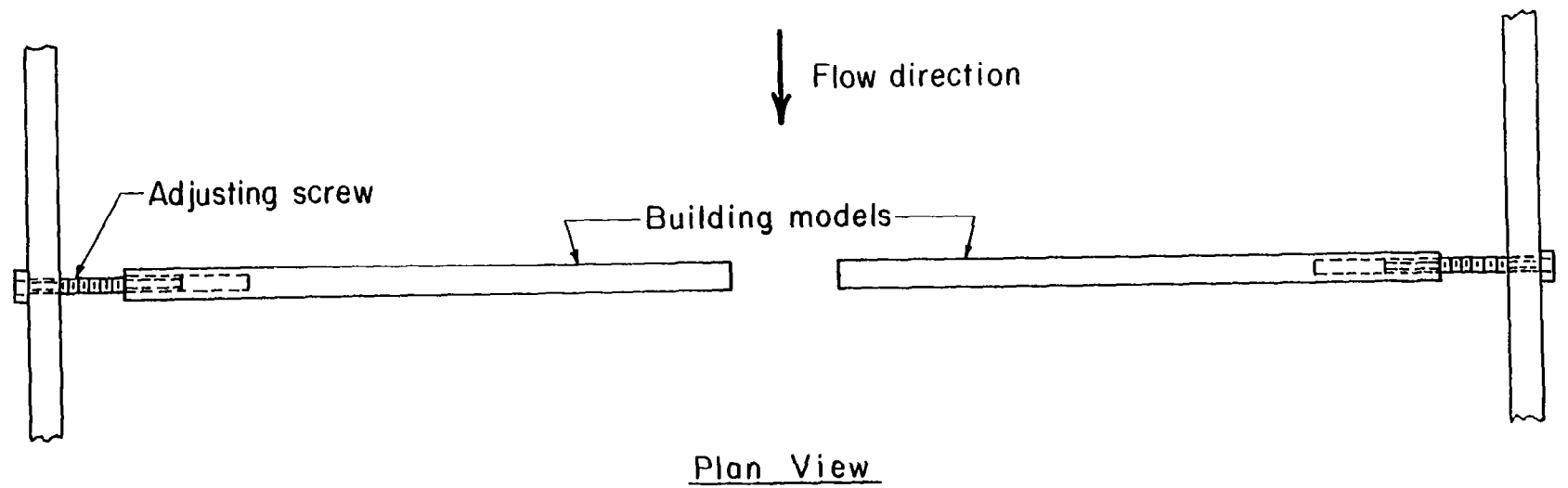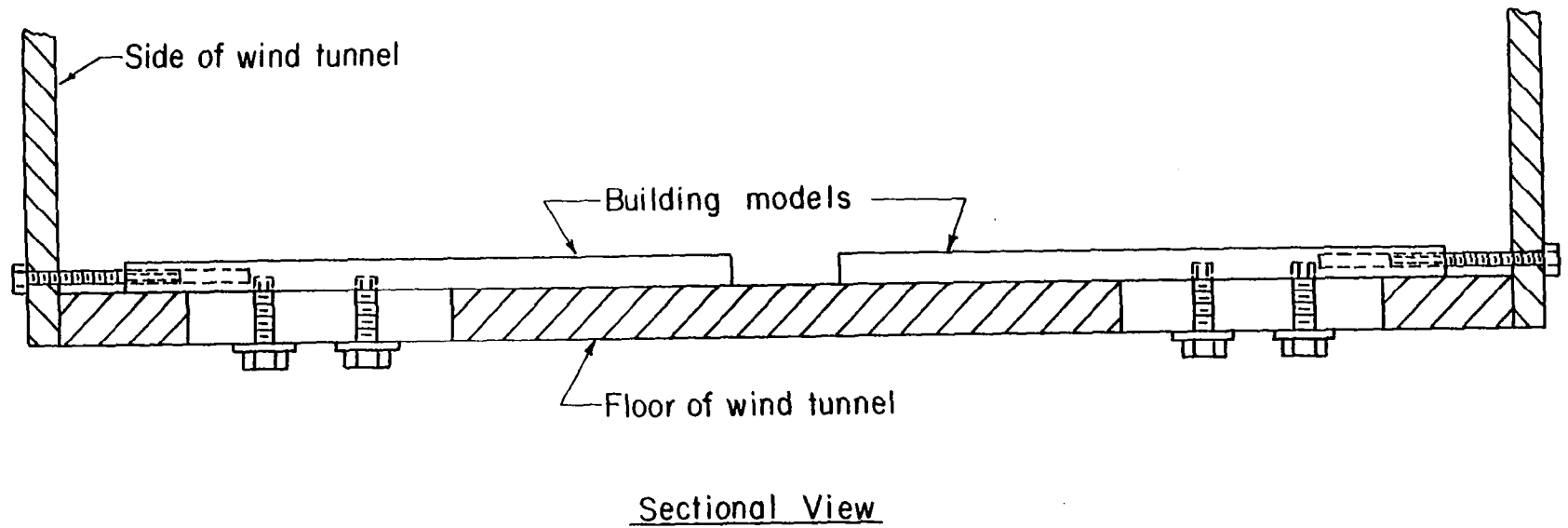
Figure I. Surface-mounted models

and wake profiles were taken along the line midway between the two ends.

A variety of obstacles have been used in previous studies available in the literature. A number of these are listed in Table 1, along with the measurements taken. The present study of the wake behind a gap in a bar-shaped model should yield profiles like the previous two-dimensional ones for the small-gap case and like the three-dimensional studies as the gap is widened. Thus the studies listed in Table 1 should be useful for comparison of results.

TABLE 1

Summary of Literature on Single Obstacles

| | Type of Obstacle | Surface | Type of Flow | Measured Quantities |
|---|---|---|---|---|
| Arie and Rouse (1956) | plate w/tail | Flat plate | 2-D | U, u', v', w' UV, $\Delta p$ |
| Mueller and Robertson (1962) Mueller, Korst and Chow (1964) | Half rounded surface | Flat plate | 2-D | U, Cp, u', UV |
| Tieleman and Sandborn (1965) | sphere | Flat plate | 3-D | U, u' Cp |
| Plate (1967) | fence | Flat plate | 2-D | U |
| Petryk and Brundrett (1967) | fence | Flat plate | 2-D | U |
| Good and Joubert (1968) | fence | Flat plate | 2-D | U, Cp |
| Chang (1966) reported by Plate (1971) | wedge | Flat plate | 2-D | U, u', v' UV |

5

| | Type of Obstacle | Surface | Type of Flow | Measured Quantities |
|---|---|---|---|---|
| Oka and Kostic (1971) | square | Flat plate | 2-D | U, V, u' |
| Castro (1971) | perforated plates | Flat plate | 3-D | U, u' |
| Sundaram, Ludwig and Skinner (1972) | fence | Flat plate | 2-D | UW, u', w' |
| Counihan (1971) reported by Woo et al. (1977) | cube | Flat plate | 2-D | U, u', v', w' UV |
| Counihan, Hunt and Jackson (1974) | square | Flat plate | 2-D | U, u', v' UV |
| Sharán (1975) | rectangular block | Flat plate | 3-D | U, u' |
| Sami and Liu (1975) | thin plate | Flat plate | 2-D | U, u', UV, $\Delta p$ |
| Castro and Robins (1977) | cube | Flat plate | 3-D | $C_p$, V, W, U, u' |
| Woo, Peterka and Cermak (1977) | rectangular block | Flat plate | 3-D | U, u' |
| Phataraphruk and Logan (1978) | rectangles | Pipe | 2-D | U, u', v', w' UV |

# CHAPTER 2

## FLOW FACILITY

In the current investigation, two bars, each with a square cross section of 8.38 mm, were placed on the floor of a smooth rectangular wind tunnel so the gap between the elements was normal to the flow. The elements were developed in order that for each gap setting the elements extended to the side wall. Five gap settings were used ranging from 0.5 to 10 times the height of the obstacle. The gap was increased until only a small effect of the elements on the flow was noticed. Air at low speeds was used as the fluid, so compressibility effects could be ignored. A Reynolds number is defined as

$$Re = \frac{U_1 H}{\nu}$$

where H is the height of the element. The Reynolds number was 3750 ($\pm$100) for all runs.

The experiment used a suction type wind tunnel (Fig. 2) which is 7.32m long, 56 cm wide and has an adjustable roof section. Plexiglas formed the sides and top while the floor was plywood laminated with a smooth formica type material. The wind tunnel was constructed in 2.44m sections then placed together at the supports and leveled. Plastic type sealer was used on the joints insuring a smooth transition. The last 2.44m of the wind tunnel was used as the test section, thus providing 4.88m in which to develop an
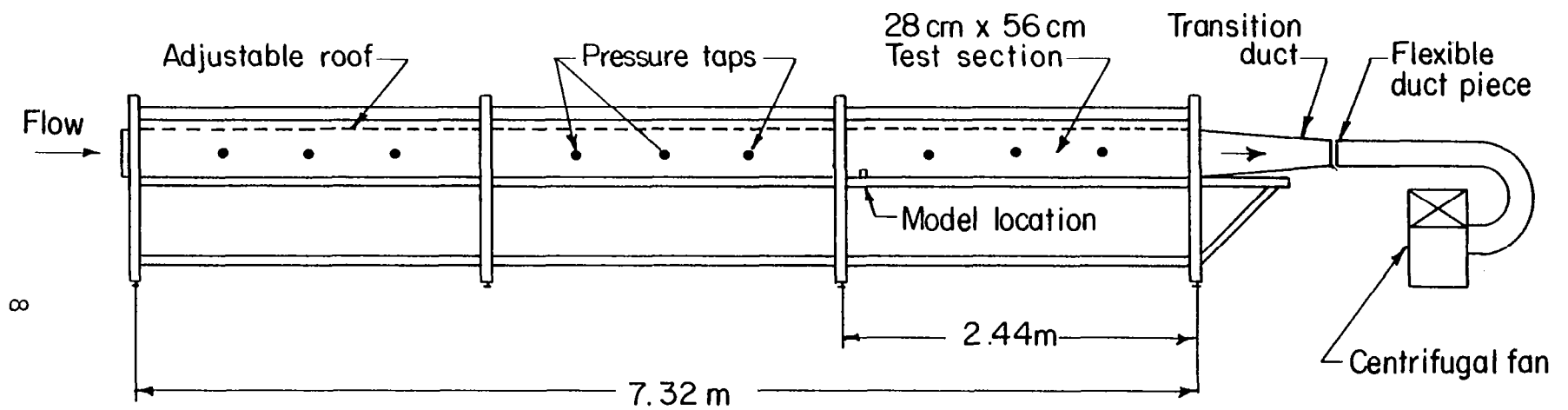
Figure 2. Schematic of wind tunnel

equilibrium boundary layer.

A diffuser and 22.8cm diameter sheet metal duct connected the wind tunnel to the suction end of a centrifugal blower. A 7.5 horsepower constant speed motor powered the blower which was set for the maximum flow rate consistent with this size motor. A short flexible duct was used to prevent the inherent blower vibrations from reaching the wind tunnel.

An ordinary furnace filter was placed at the entrance of the wind tunnel to filter out any dust particles which might break the hot-wire probes or make them dirty. A honeycomb type flow straightener was located directly behind the filter. It had a 1:8 diameter to length ratio which is within a standard usage range (Petryk and Brundret, 1967). A 12.7mm high piece of quarterround wood was placed normal to the flow and the width of the wind tunnel approximately 15 cm down stream from the flow straightener. This "tripped" the flow to increase the boundary layer height. Downstream from the trip was placed 60 cm of number 16 sandpaper to increase turbulence.

The roof of the wind tunnel was adjusted for a zero pressure gradient and its height above the floor ranged from 25.4 cm at the entrance to 29.9 cm at the blower end. Pressure taps were located on the sides of the wind tunnel as shown in Fig. 2 in order to insure equal static pressures. These pressure taps were designed with negligible error according to Benedict (1977).

In order to allow the probes to be inserted into the flow, portions of the top of the test section were cut with slots. During data taking,

9

all the slots were closed except the slot where the probe was located so that the inside top surface was nearly smooth. A special slot cover was designed to insure only minor leakage around the probe and minimal disturbance to the flow.

A traversing-and-elevating device was designed to allow accurate placement of the probe and the ability to move the probe in any direction. The stand for the traversing-and-elevating device could be moved lengthwise along the wind tunnel, thus insuring the probe could be inserted into any portion of the test section. There were two probe holders separated by a distance of one inch which provided the ability to calibrate the hot-wire probe within the wind tunnel.

The models were constructed of aluminum and cut to within ± 0.01 mm tolerance. Each element was 23.5 cm long and was attached to the wind tunnel floor with bolts as shown in Fig. 1. The gap was adjusted by placing an aluminum block of the correct size between the elements and using the adjustment screws to make minor changes. The models were then tightened into position and the adjustment block removed. Modeling clay was placed over the adjustment screws and shaped like the roughness elements to insure no end effects were measured in the flow downstream.

Mean velocity profiles in the turbulent boundary were measured by Pitot tubes and the hot wire anemometer technique. Both profiles were compared with that from Klebanoff and Diehl (1951) and Wieghardt (1953) to insure that the techniques were giving correct results. The longitudinal turbulence intensity was also measured with the hot wire and for this reason it was preferred over the Pitot tube. Measurements were made

10

only along the centerline of the wind tunnel, thus effects of the walls and lateral velocity components could be neglected.

Pitot tube and static port measurements were made with a Meriam Model 34FB2 Micromanometer. This allowed a reading to within 0.01 mm of water.

A normal hot wire probe (DISA 55P11) was used to measure mean velocities and longitudinal turbulences. The wire was 5μm in diameter and 1.25 mm long. The probe was inserted from the wind tunnel top with the probe supports normal to the flow. In this way, measurements could be made closer to the floor.

A constant temperature anemometer (DISA 55 D01) was used with the normal probe, and the output was electronically linearized (DISA 55 D10). The linearized mean velocities were read on a D.C. voltmeter (DISA 55 D30). The root-mean-square values of the fluctuating components were read on a R.M.S. voltmeter (DISA 55D 35).

The hot wire was calibrated with a standard 3.2 mm outside diameter Pitot tube. Both the hot wire and the Pitot tube were located at the same point above the floor and longitudinally, but were 25 mm apart laterally. Due to the difficulties with low velocity flow, the linearizer exponent was determined from an air flow near the end of a two inch diameter nozzle. The flow from the nozzle was capable of a velocity of 110 feet per second. The exponent was checked and calibration made in the wind tunnel using two different velocities. Care was taken to insure that the lower velocity was higher than 16 fps which, according to DISA instructions, the calibration becomes unreliable. The hot wire was recalibrated every

11

three hours in order to avoid any errors due to the drift of the electronic equipment. Since dirt deposition on hot wires has a very important effect on the accuracy of the measurement, the wire was checked by microscope if a change in the exponent was noticed.

The uncertainty of this experiment is shown in the Appendix to explain the possibility of error in the experiment.

CHAPTER 3

EXPERIMENTAL RESULTS

Measurement of longitudinal mean velocity and longitudinal turbu-
lence intensity in an equilibrium boundary layer developed over a smooth
channel was the first part of the experimental work. The second part in-
volved these measurements behind a single element and comparison with the
two-dimensional profiles of other experimentalists. The measurement of
longitudinal mean velocity and longitudinal turbulence intensity in the
flow downstream from the gaps between the elements of .5, 1, 1.5, 5 and 10
times the element height was then undertaken, completing the centerline
experiments. Eleven downstream measuring stations were used ranging from
one at the rear of the element to a point 224 element heights downstream.

FLOW IN THE SMOOTH CHANNEL

Longitudinal mean velocity was measured both by a standard Pitot tube
and by a hot wire normal probe. The results of these measurements were
compared against those made by Wieghardt (as presented by Coles and Hirst,
1969) and Klebanoff and Diehl (1951), as shown in Fig. 3. Coles tabulated
Wieghardt's flow over a flat plate according to the Reynolds number based
on the momentum thickness as the length parameter. Using a summation type
of integration for calculation of the momentum thickness for both the pre-
sent Pitot-tube and hot-wire boundary layer measurements, the Reynolds
number was determined to be 2490. Wieghardt's data for a Reynolds number
of 2397.8 was found to be the nearest to this value. Klebanoff and Diehl's
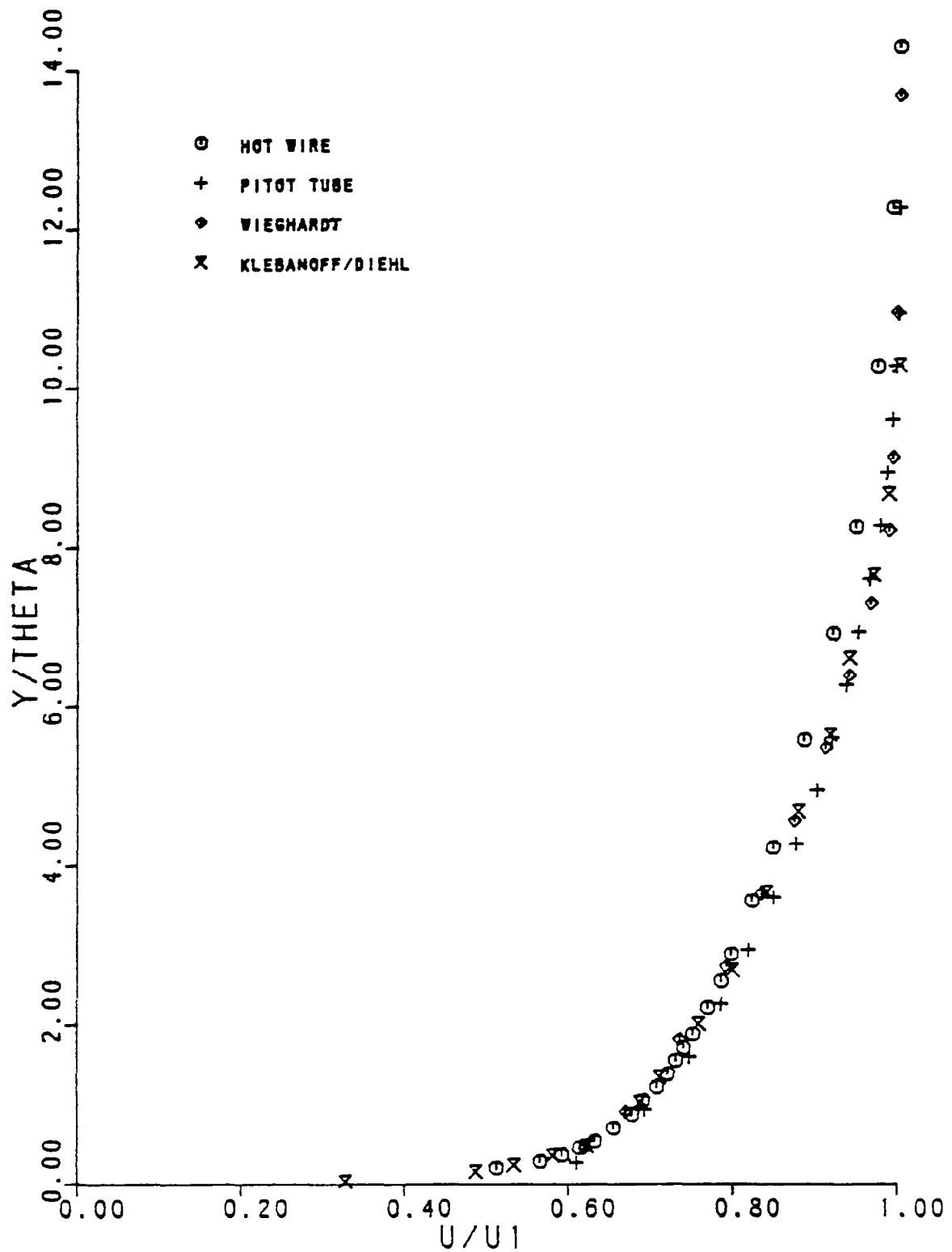(1951) data were collected from equilibrium flow downstream from number 16

Fig. 3    Comparison of Mean Velocity Profiles for
Smooth Channel Flow.

14

sandpaper placed on a flat plate. Using the momentum thickness as the non-dimensionalizing factor for the height above the floor, the comparison generally shows good agreement especially in the region nearest the floor.

The root-mean-square of the longitudinal turbulence intensity measured by the hot wire normal probe is compared agianst the results of Klebanoff and Diehl (1951) in Fig. 4. Disagreement in the graphs near the free stream is caused by differences in free stream turbulence level in the two wind tunnels. The disagreement of the turbulence intensity nearest the floor is caused by the difference in upstream history between the flows compared. A smooth channel boundary layer profile in a semi-logarithmic plot is shown in Fig. 5 and may be used as a comparison to the follow-on graphs of flows interrupted by the roughness elements.

## FLOW BEHIND A SINGLE OBSTACLE

A single obstacle, or roughness element, was formed when the gap between the two elements was reduced to zero. Since each element was of equal size, a two-dimensional obstacle to the flow could then be produced. Figs. 6 through 8 show the longitudinal mean velocity profiles at various stations downstream in a semi-logarithmic plot. The longitudinal component of mean velocity U is non-dimensionalized with respect to the free stream velocity $U_1$, and the distance above the floor Y is non-dimensionalized with respect to the height H of the element. The stations of velocity profile in each figure are based on the non-dimensionalized distance x from the back face of the element with respect to the height H of the roughness element.

These longitudinal mean velocity profiles were compared with Good and Joubert (1968), Oka and Kostic (1971), and Phataraphruk and Logan (1978).
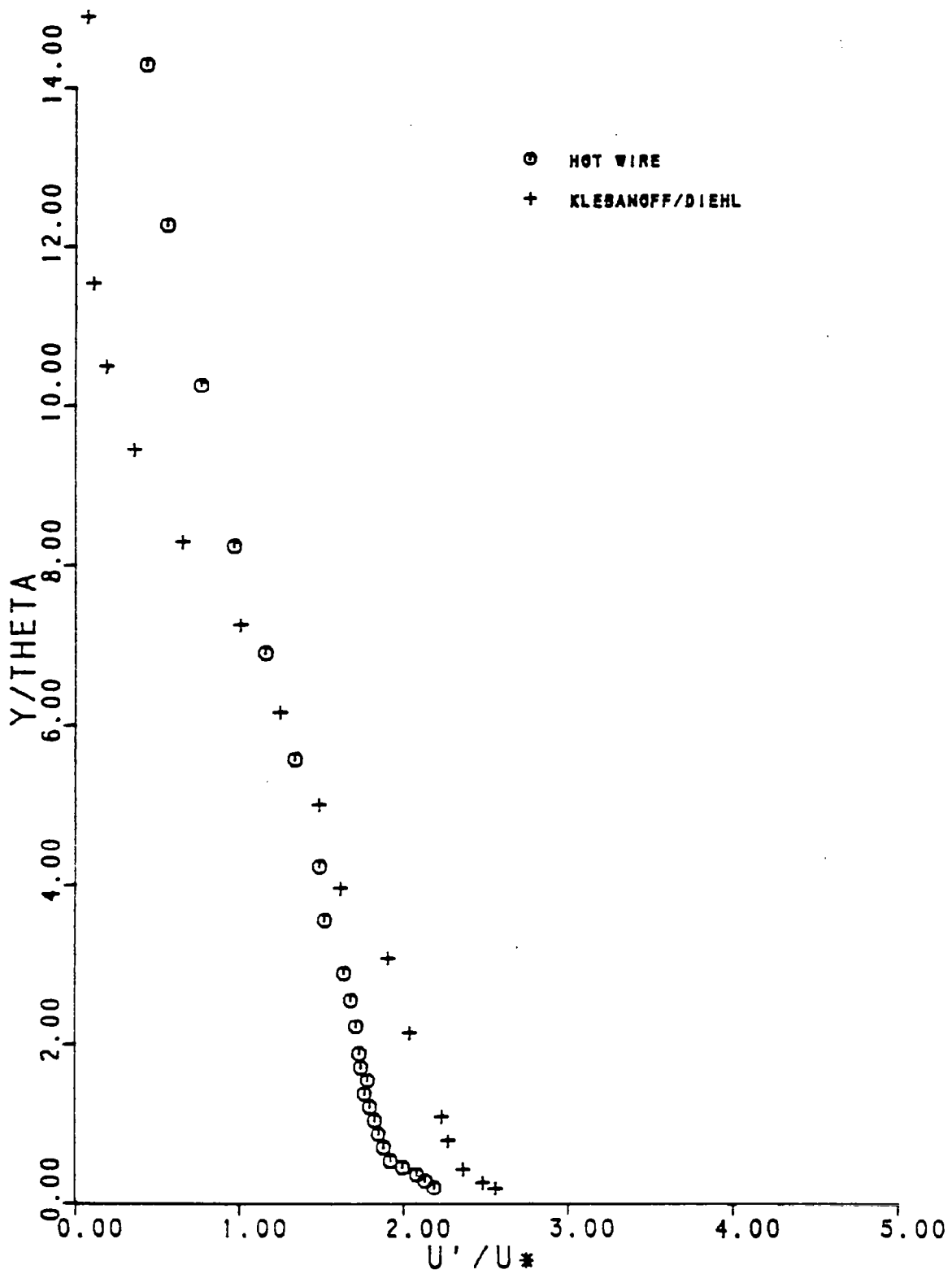
15

Fig. 4    Comparison of Longitudinal Turbulence Intensity
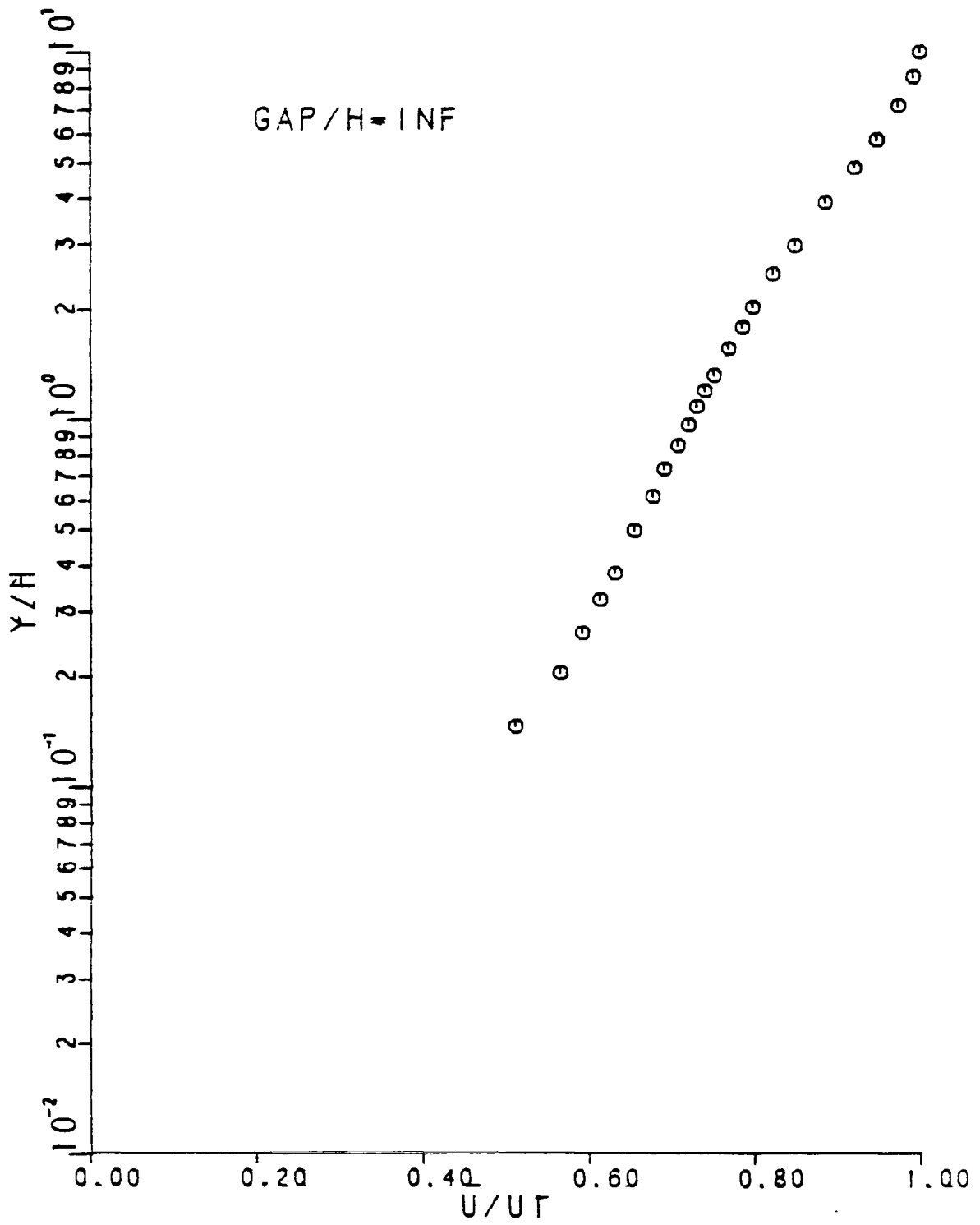for Smooth Channel Flow.
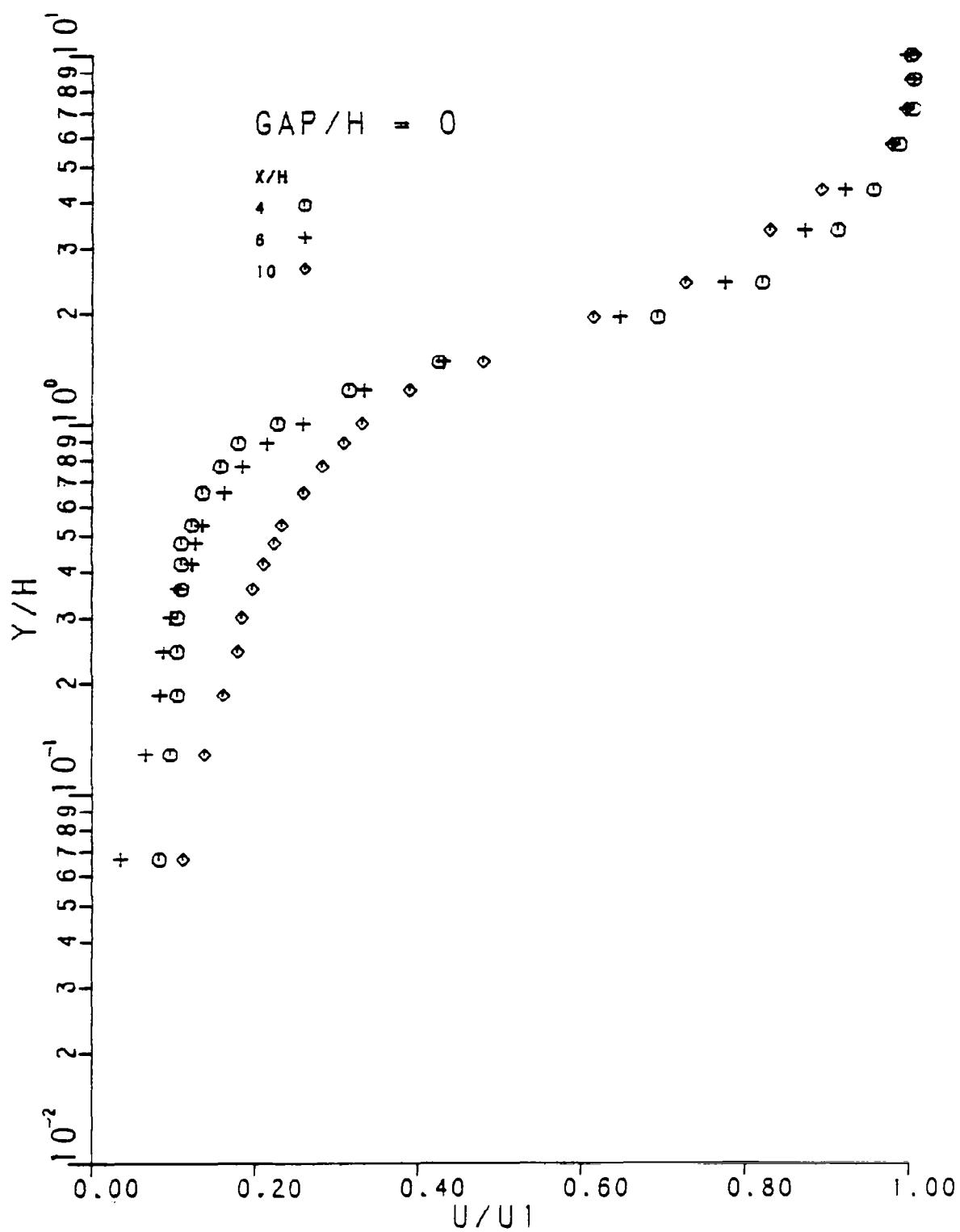
Fig. 5    Mean Velocity Profile for Smooth Channel Flow.
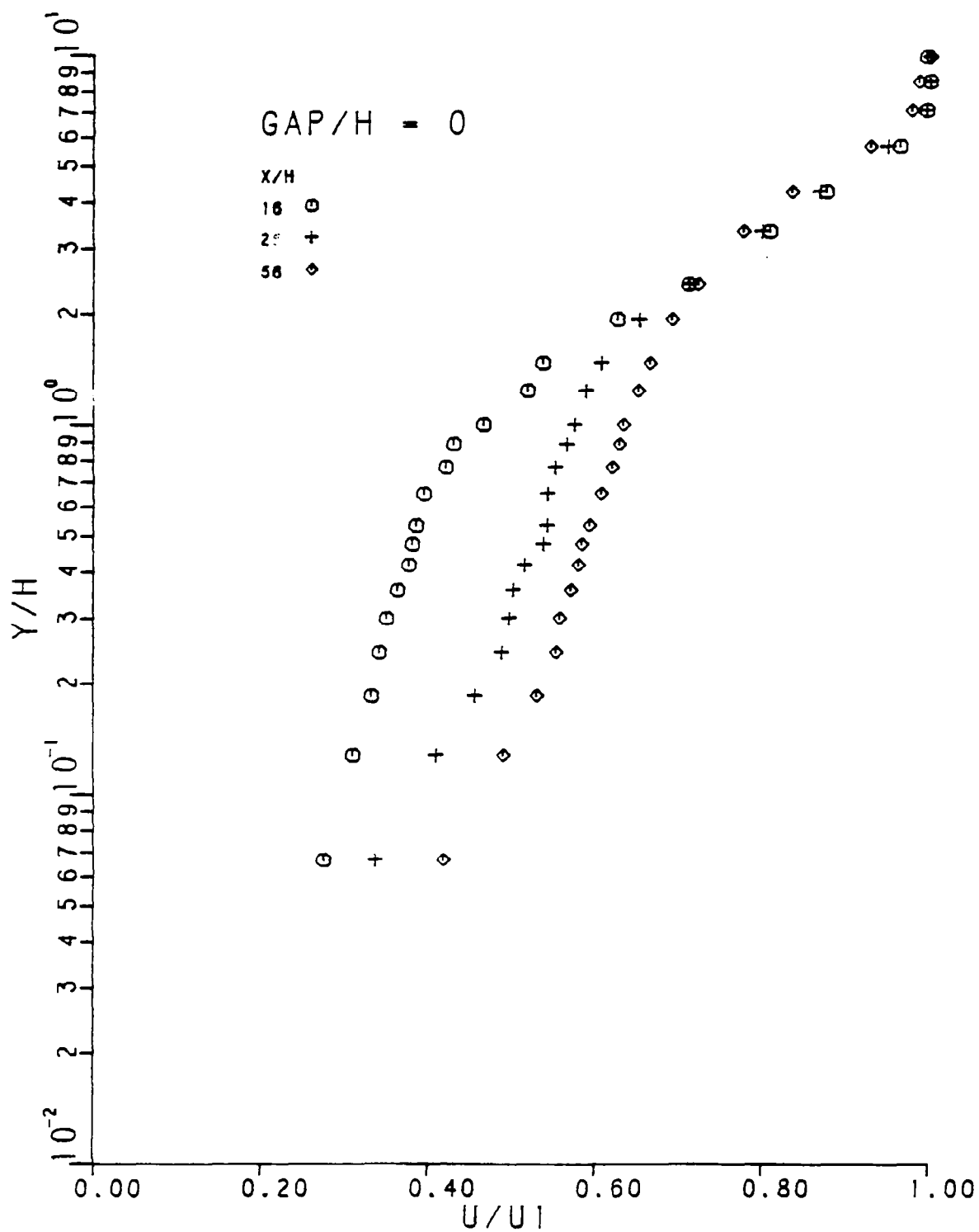
17

Fig. 6 Mean Velocity Profiles GAP/H=0, x/H=4, 6, 10.

18

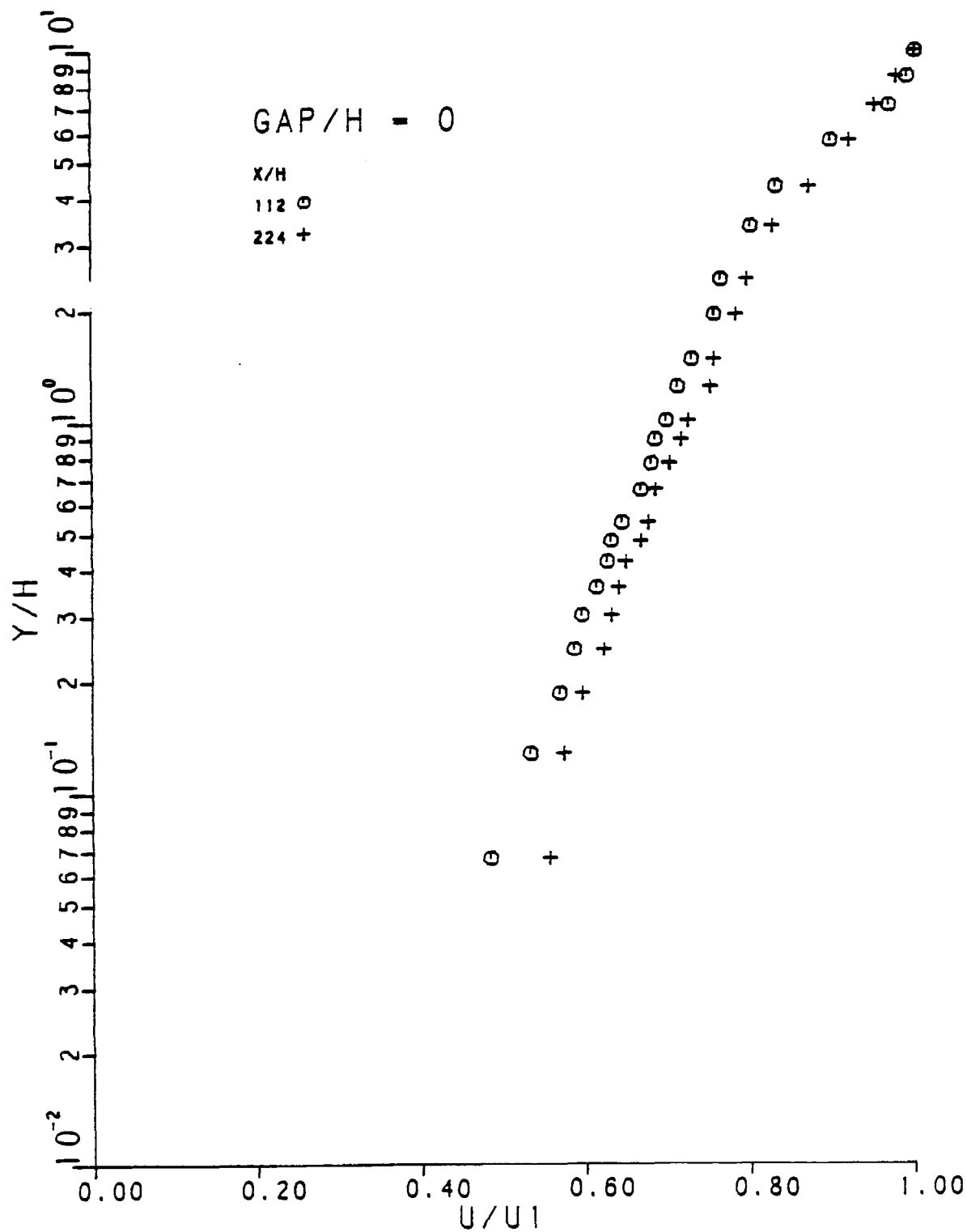Fig. 7    Mean Velocity Profiles    GAP/H=0, x/H=16, 28, 56.

19

Fig. 8    Mean Velocity Profiles    GAP/H=0, x/H=112, 224.

The present work was found to be in agreement with the earlier experimentalists.

The longitudinal turbulence intensity for the single roughness element is shown for the downstream locations in Figs. 9 through 11. The root-mean-square of the longitudinal turbulence intensity $U'$ is non-dimensionalized with respect to the smooth channel friction velocity $U^*$. These were compared with the results of Phataraphruk and Logan (1978) and found to be in agreement. As described by Oka and Kostic (1971), there is a difficulty in measuring velocities accurately in the recirculation region directly behind the roughness element with a single hot wire probe. The major problem was that the direction of flow could not be determined precisely since the hot wire anemometer read only the resultant velocity in this region.

## FLOW BEHIND GAPS BETWEEN TWO MODELS

The longitudinal mean velocity profiles for the flow behind gaps between two elements are shown in Figs. 12 through 22. These are non-dimensionalized similar to the mean velocity profiles using a single element. According to Oka and Kostic (1972), there is a wall effect on the hot wire anemometer reading when $YU^*/\nu$ is less than 5. However, Thinh (1969) found that for a normal probe placed 90° to a flow there was a wall effect when $YU^*/\nu$ is less than 10. Since the probe in this experiment was inserted 90° to the flow, the minimum distance above the wall must be 0.559 mm to satisfy Thinh's criteria. This was then selected as the lowest point of measurement for each profile.

The root-mean-square of the longitudinal turbulence intensity for downstream locations is shown in Figs. 23 through 33. These are non-dimensionalized in a manner similar to the turbulence intensity for a single element.
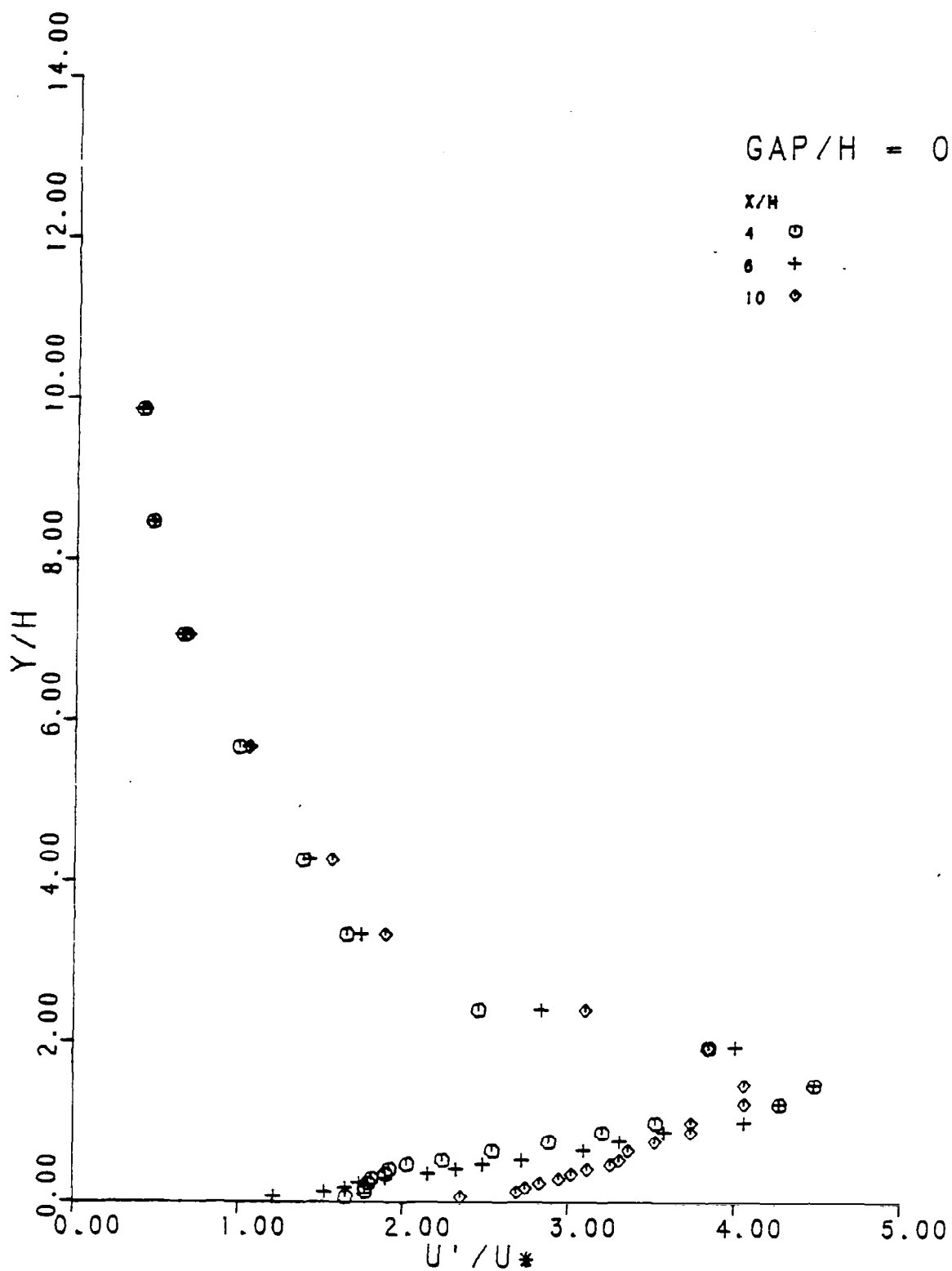
21

Fig. 9  Longitudinal Turbulence Intensity GAP/H=0, x/H=4, 6, 10.
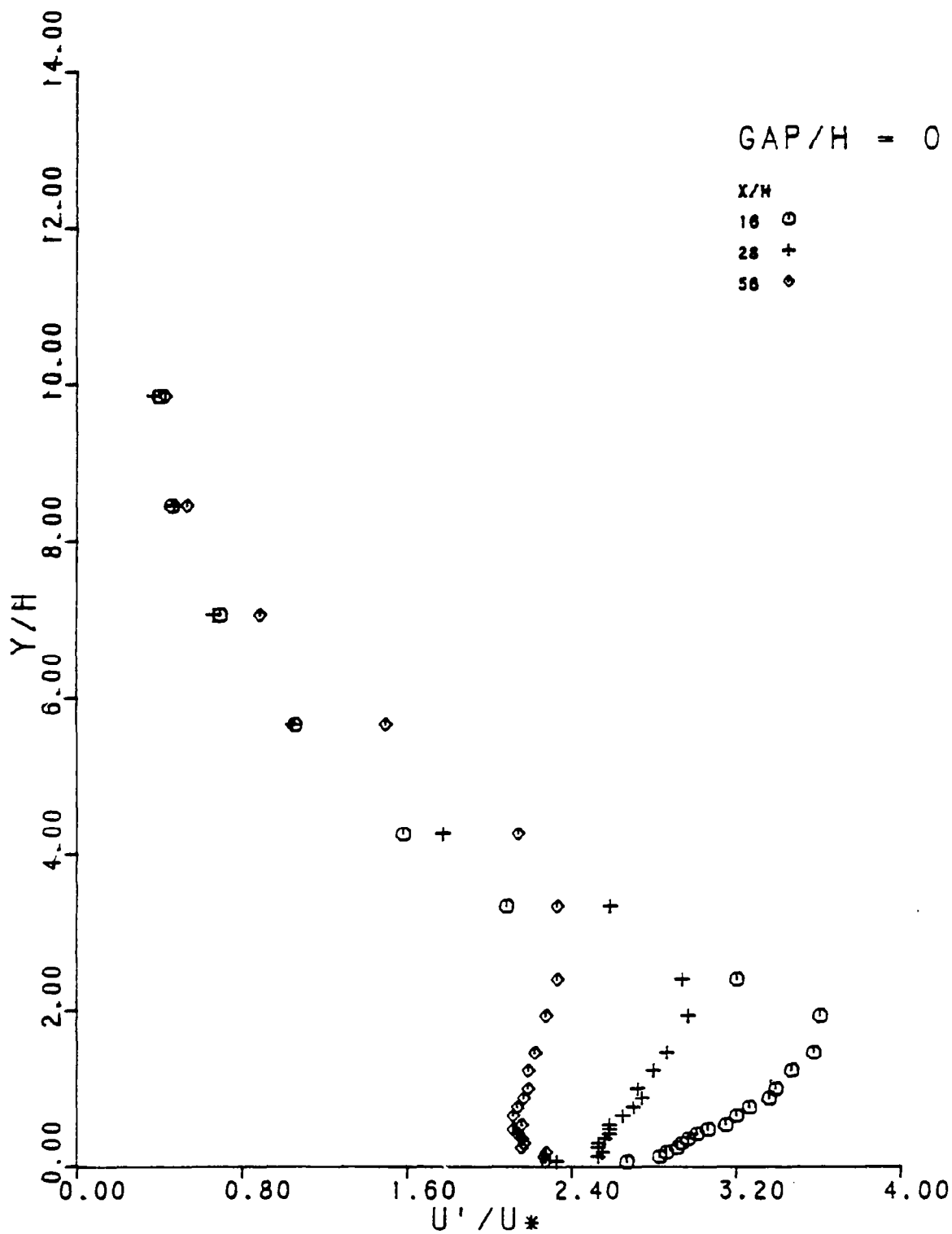
Fig. 10    Longitudinal Turbulence Intensity GAP/H=0, x/H=16, 28, 56.
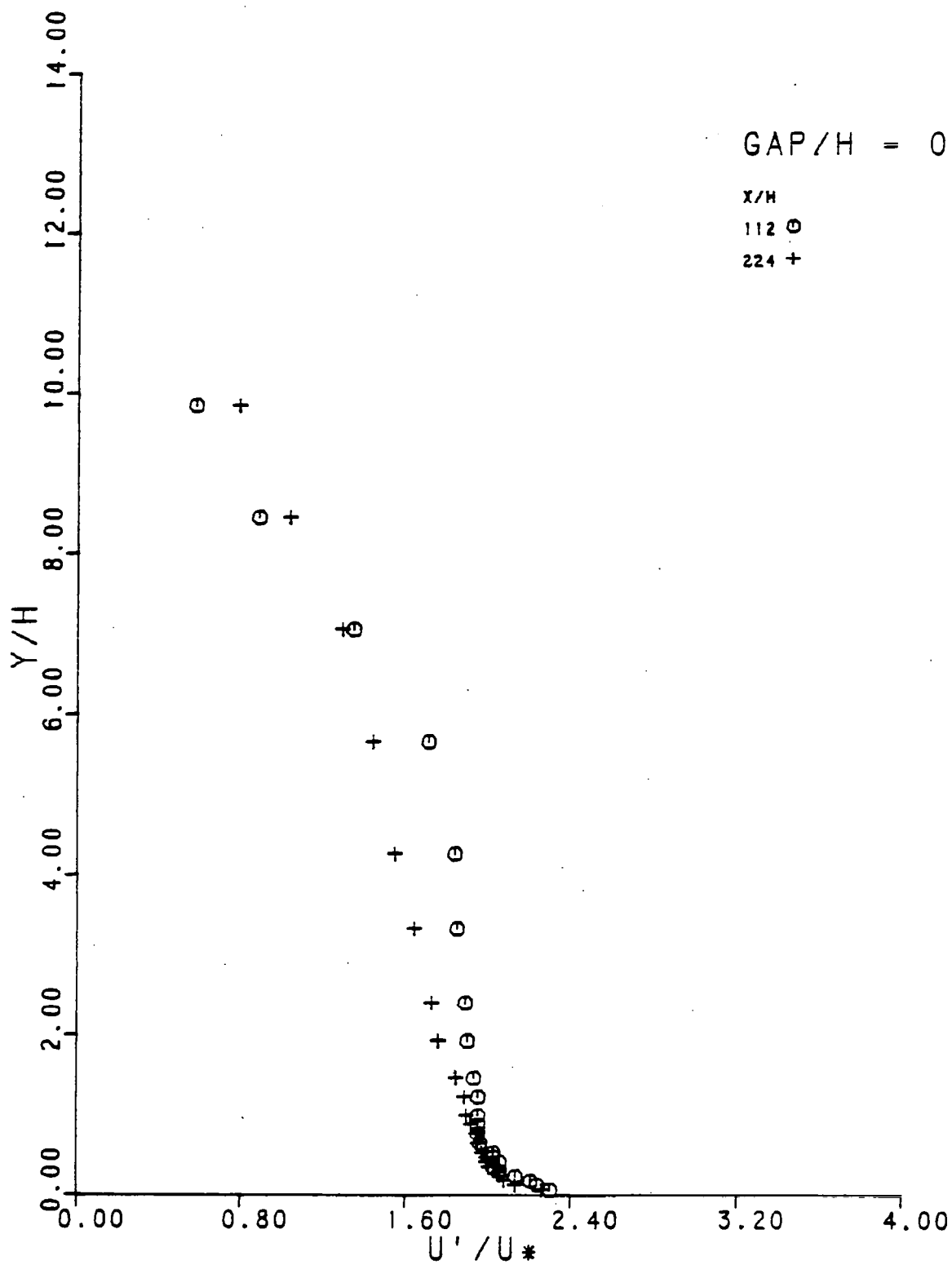
Fig. 11    Longitudinal Turbulence Intensity GAP/H=0,  x/H=112, 224.

24

Fig. 12    Comparison of Mean Velocity Profiles, x/H = 0.

25

Fig. 13    Comparison of Mean Velocity Profiles, x/H = 1.

26
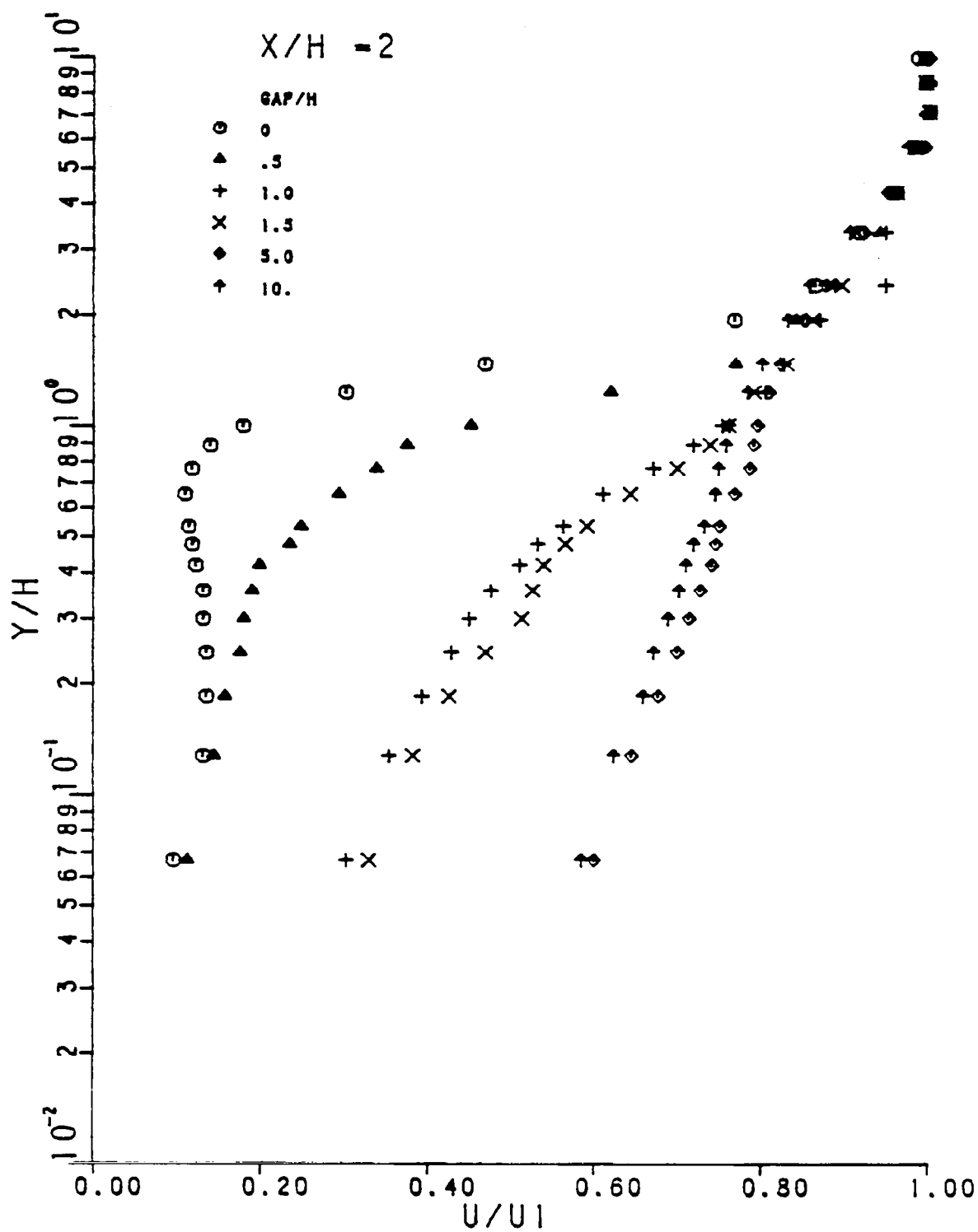
Fig. 14   Comparison of Mean Velocity Profiles, x/H = 2.

27
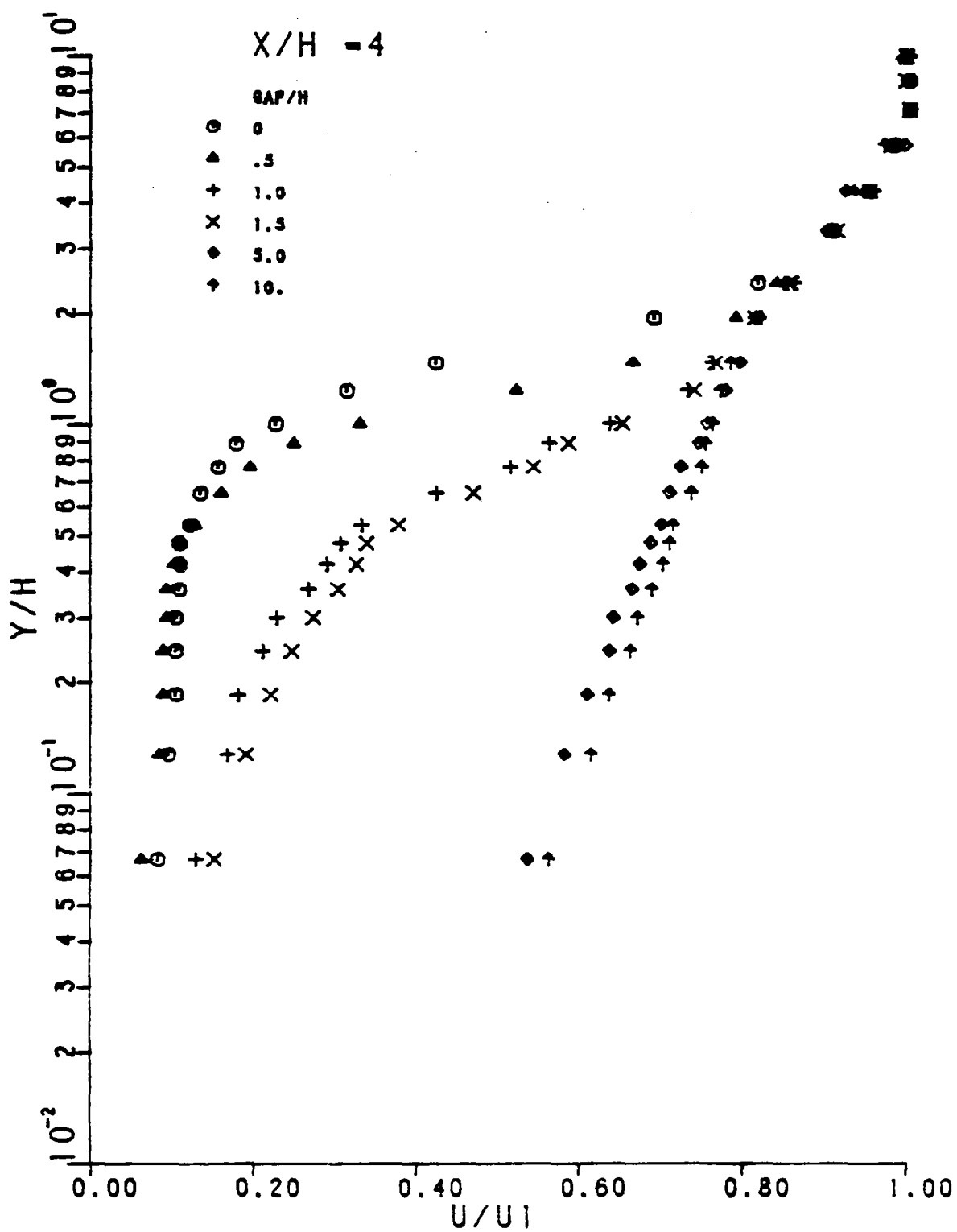
Fig. 15    Comparison of Mean Velocity Profiles, x/H = 4.

28
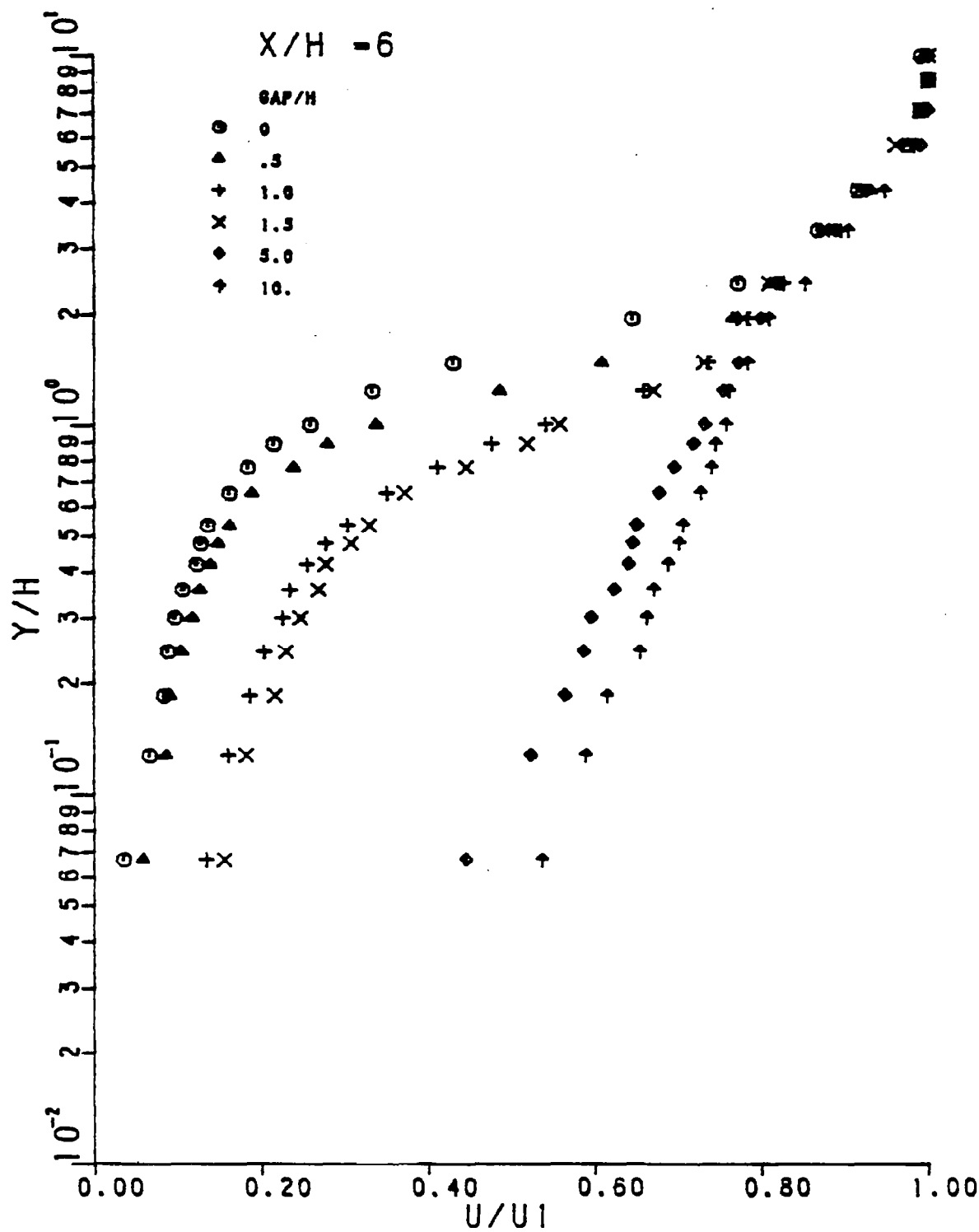
Fig. 16    Comparison of Mean Velocity Profiles, x/H = 6.
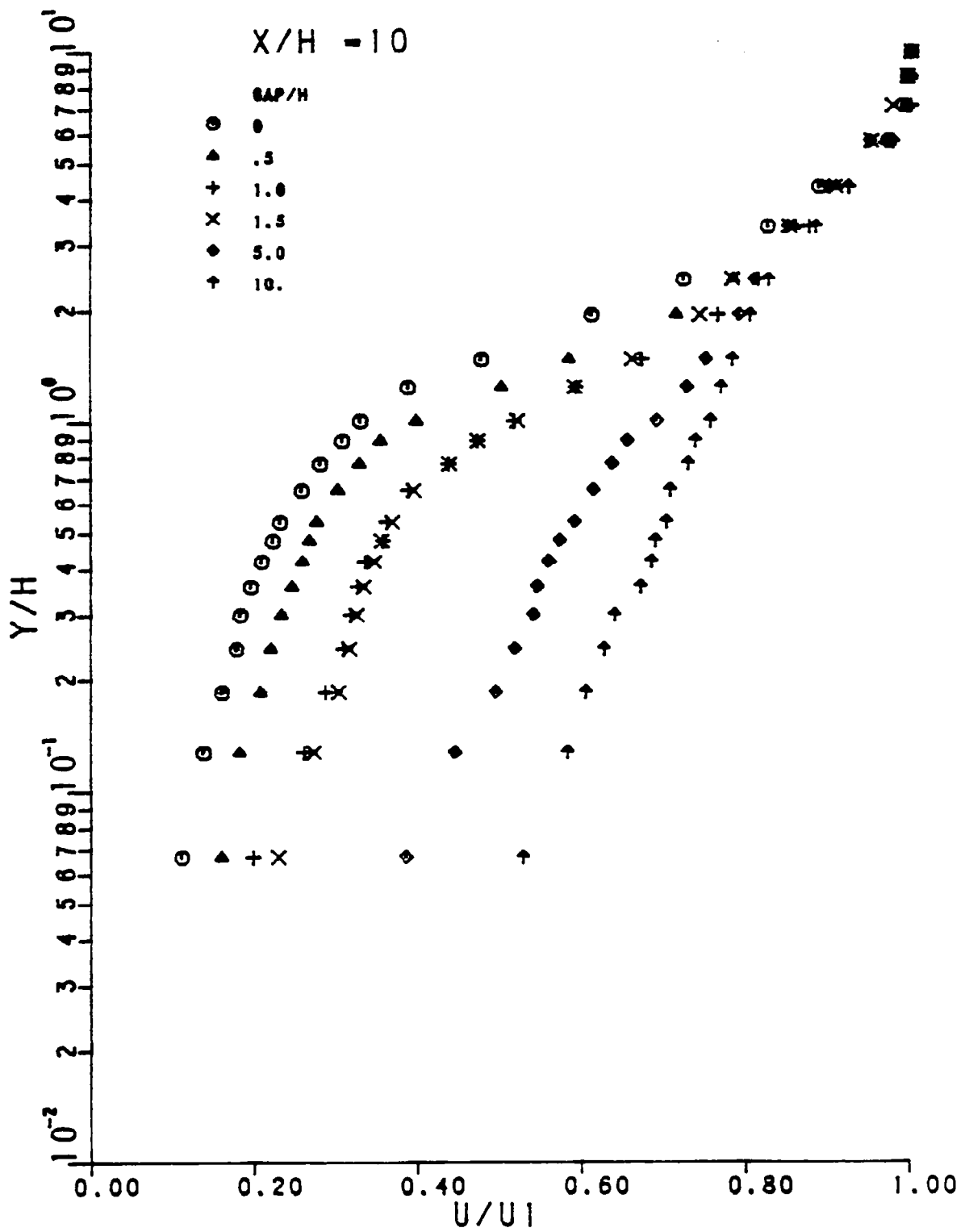
Fig. 17    Comparison of Mean Velocity Profiles, x/H = 10.
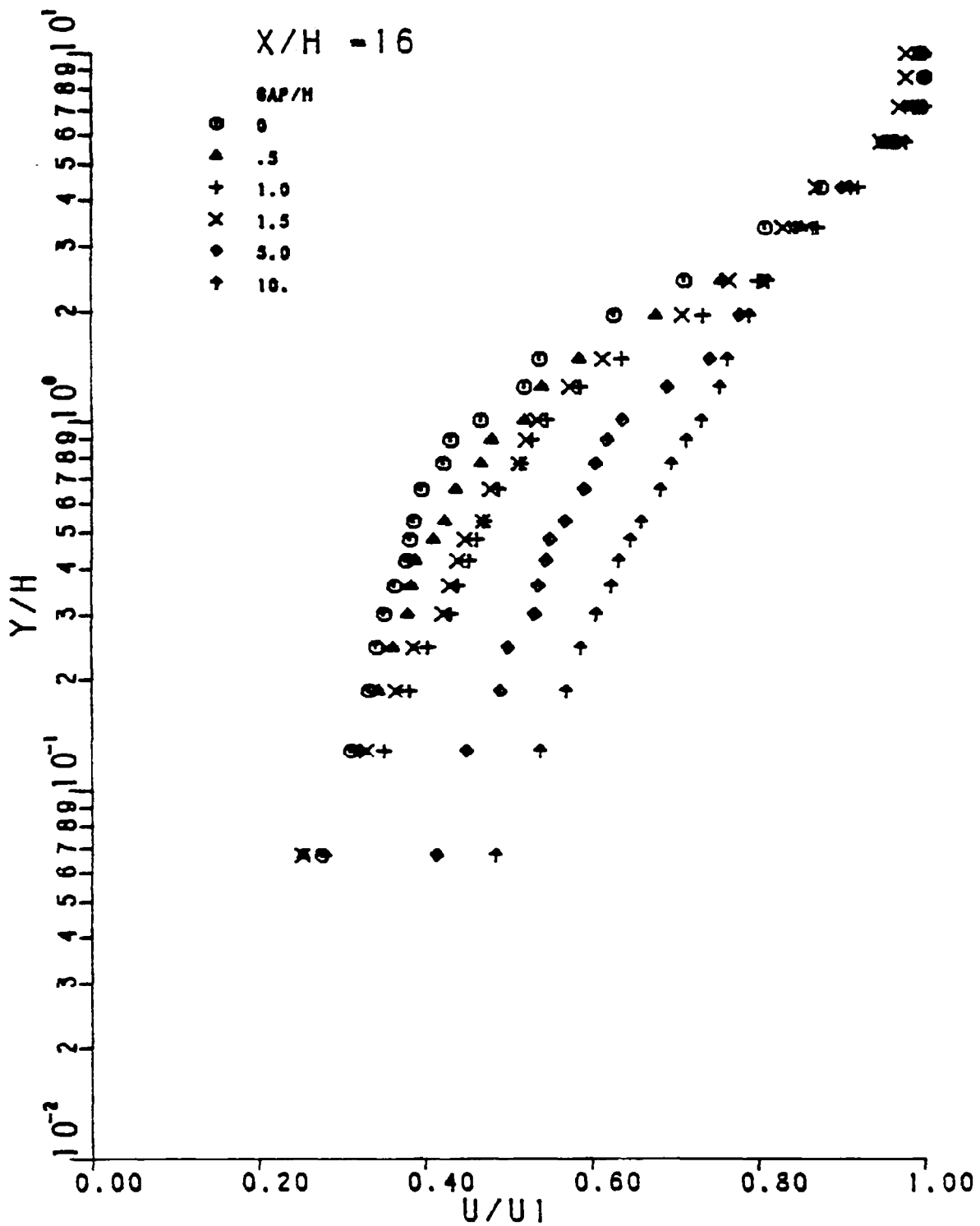
Fig. 18    Comparison of Mean Velocity Profiles, x/H = 16.
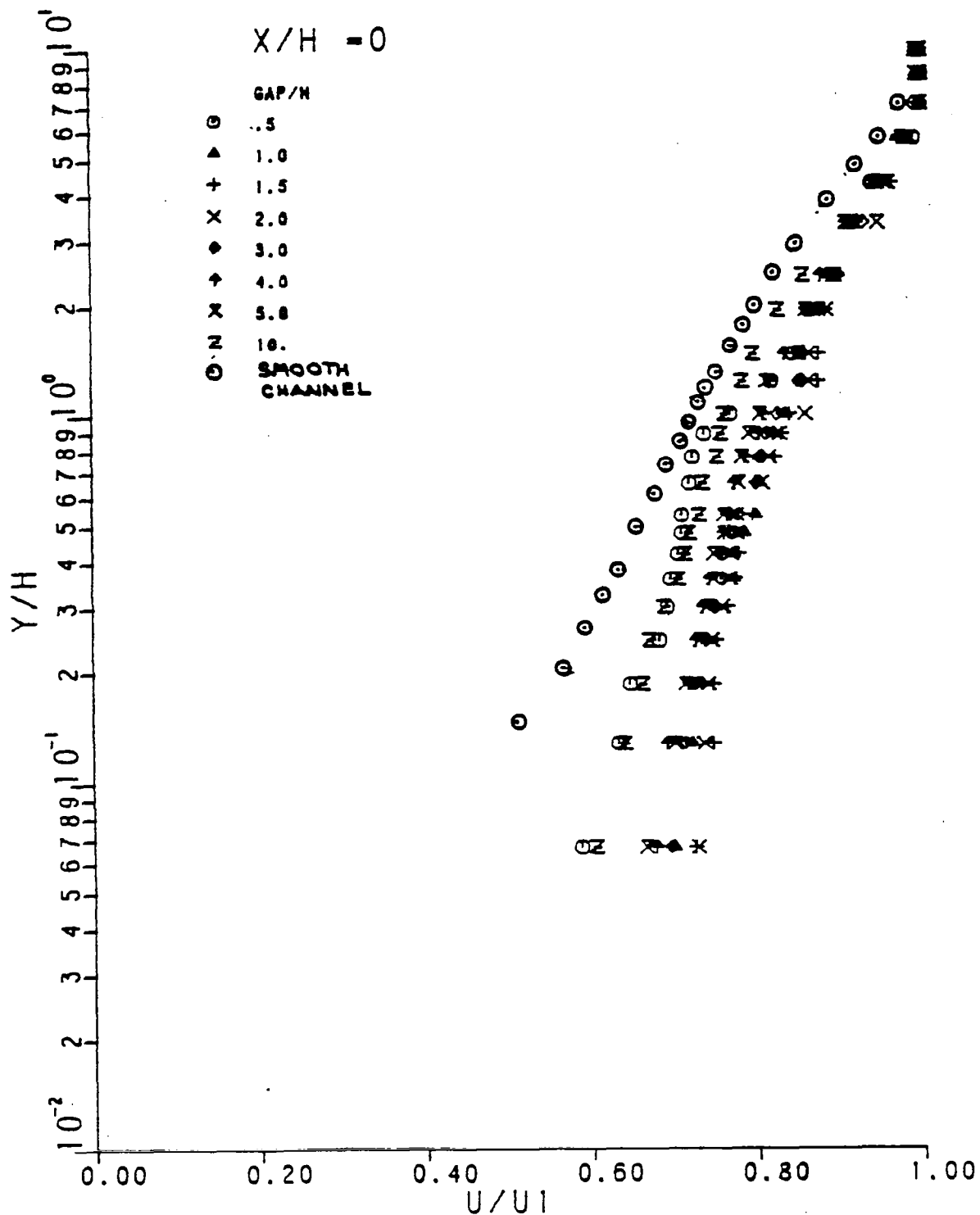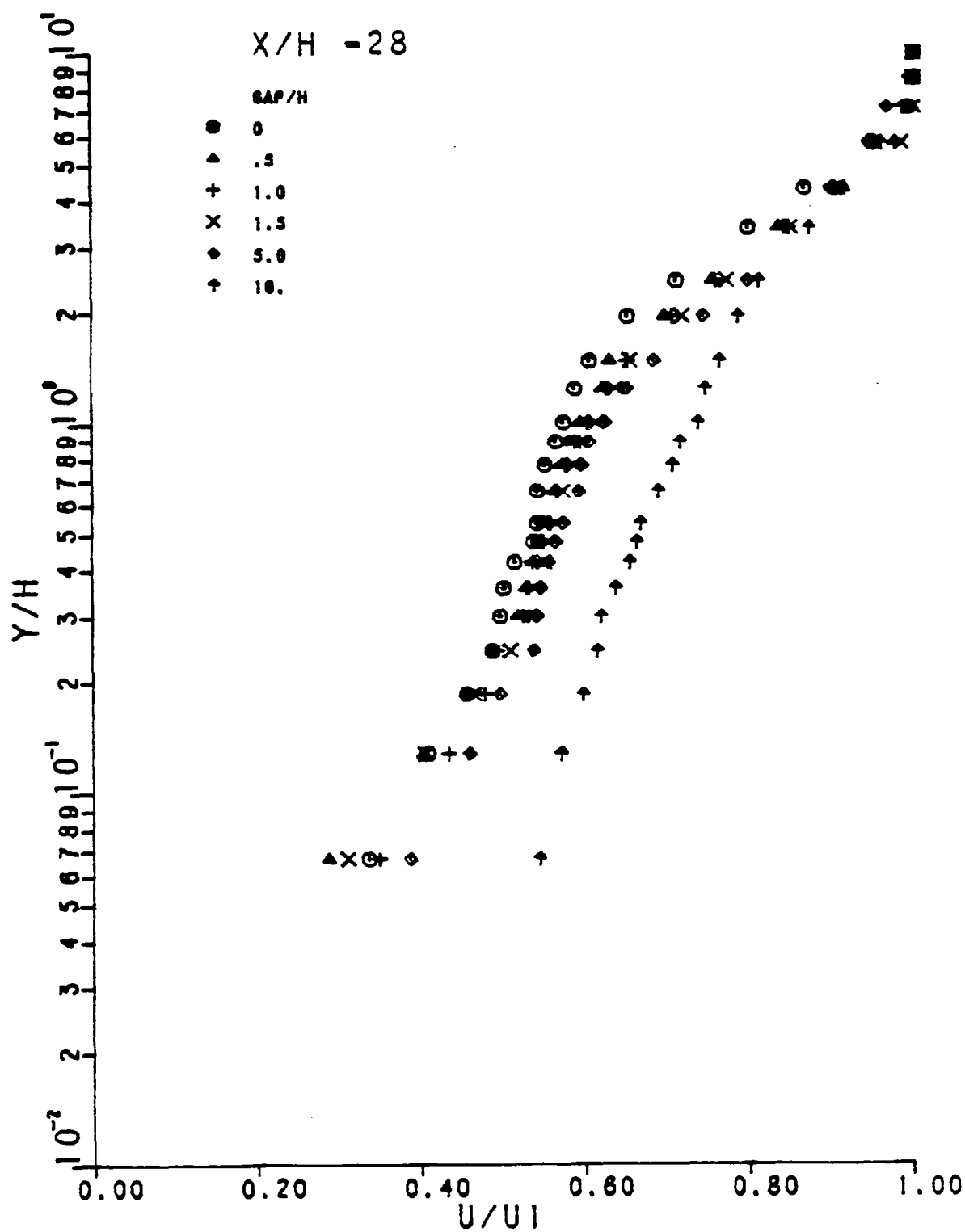
Fig. 19    Comparison of Mean Velocity Profiles, x/H = 28.

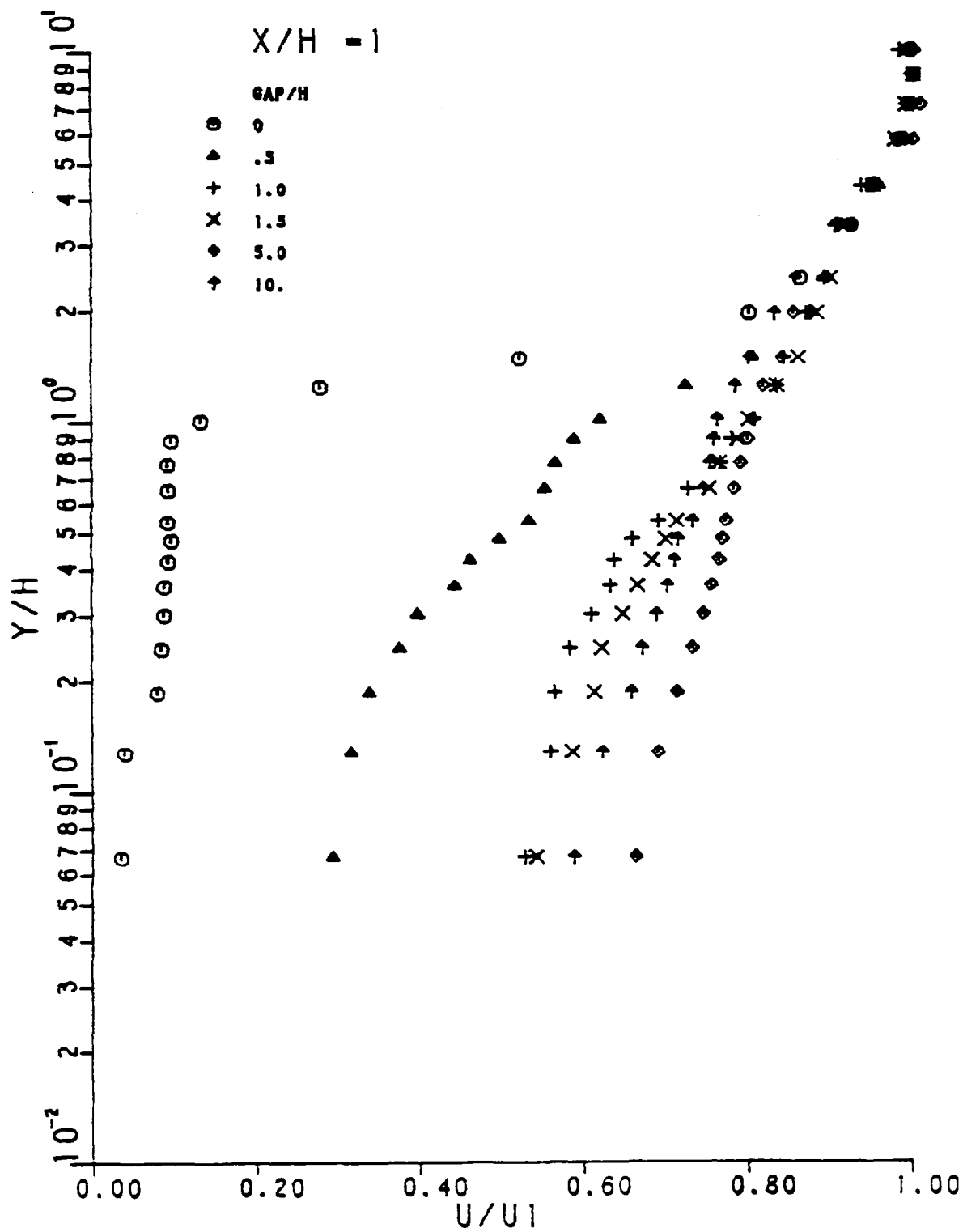Fig. 20    Comparison of Mean Velocity Profiles, x/H = 56.

33
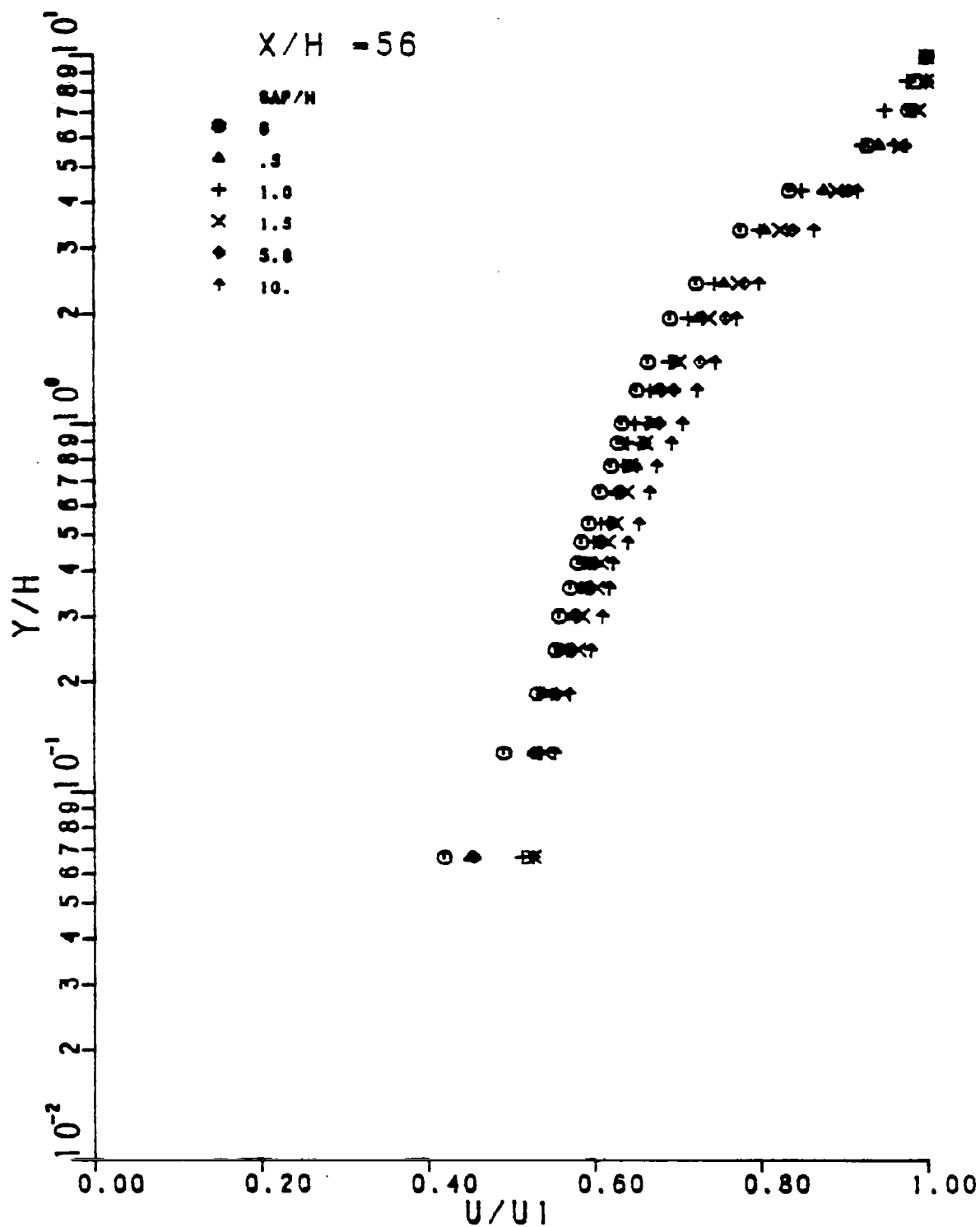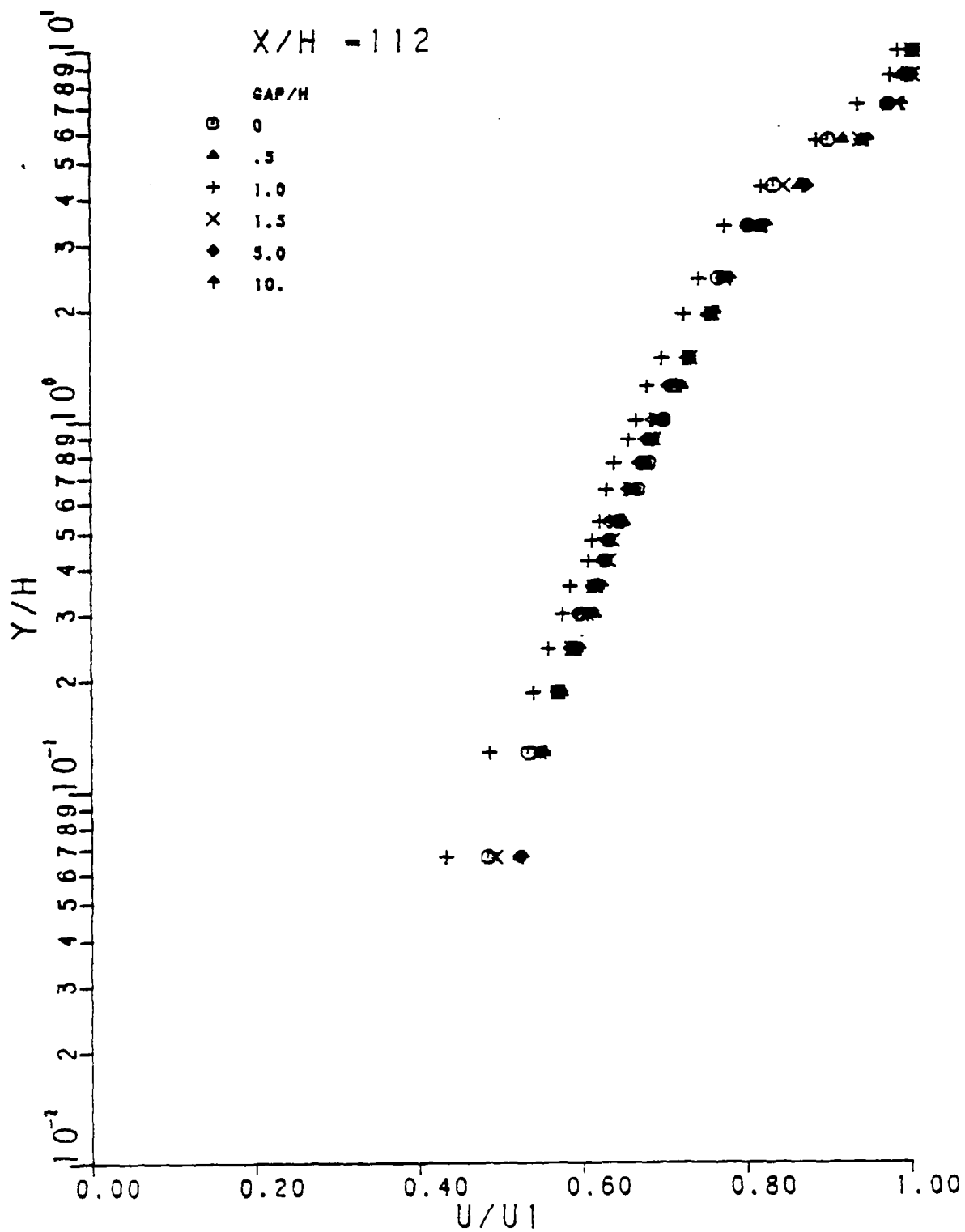
Fig. 21     Comparison of Mean Velocity Profiles, x/H = 112.

34
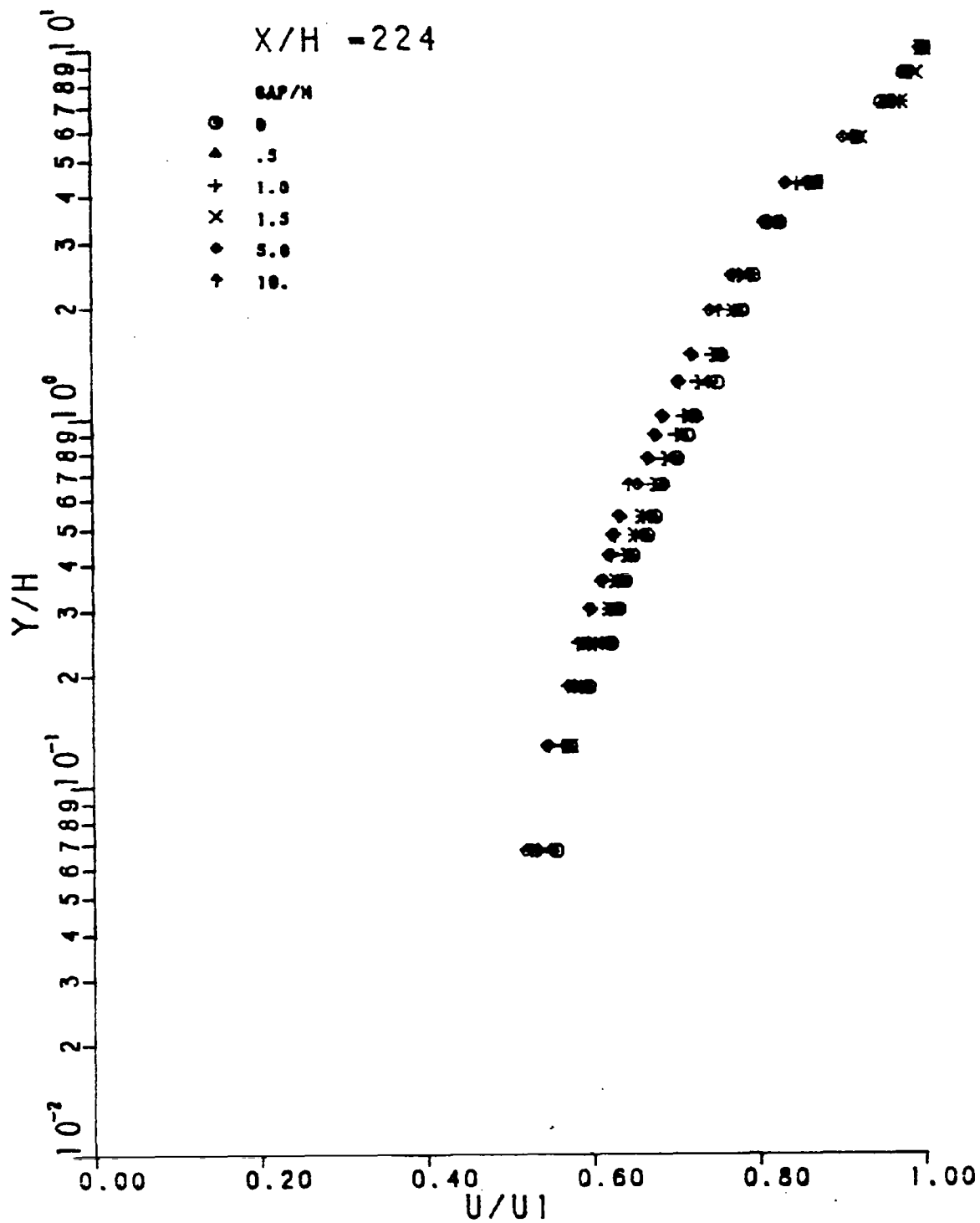
Fig. 22 Comparison of Mean Velocity Profiles, x/H = 224.
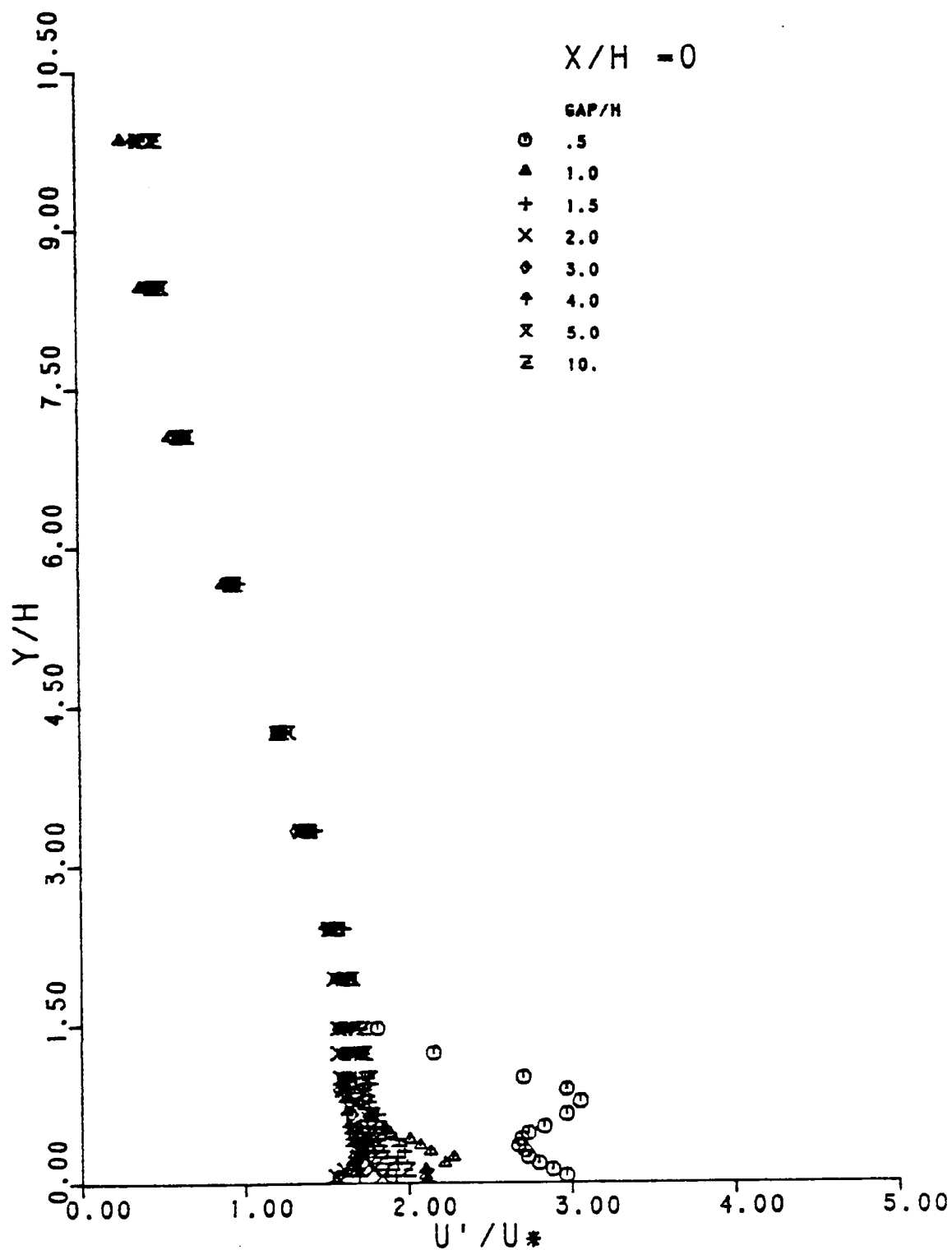
Fig. 23    Comparison of Longitudinal Turbulence Intensity, x/H=0.
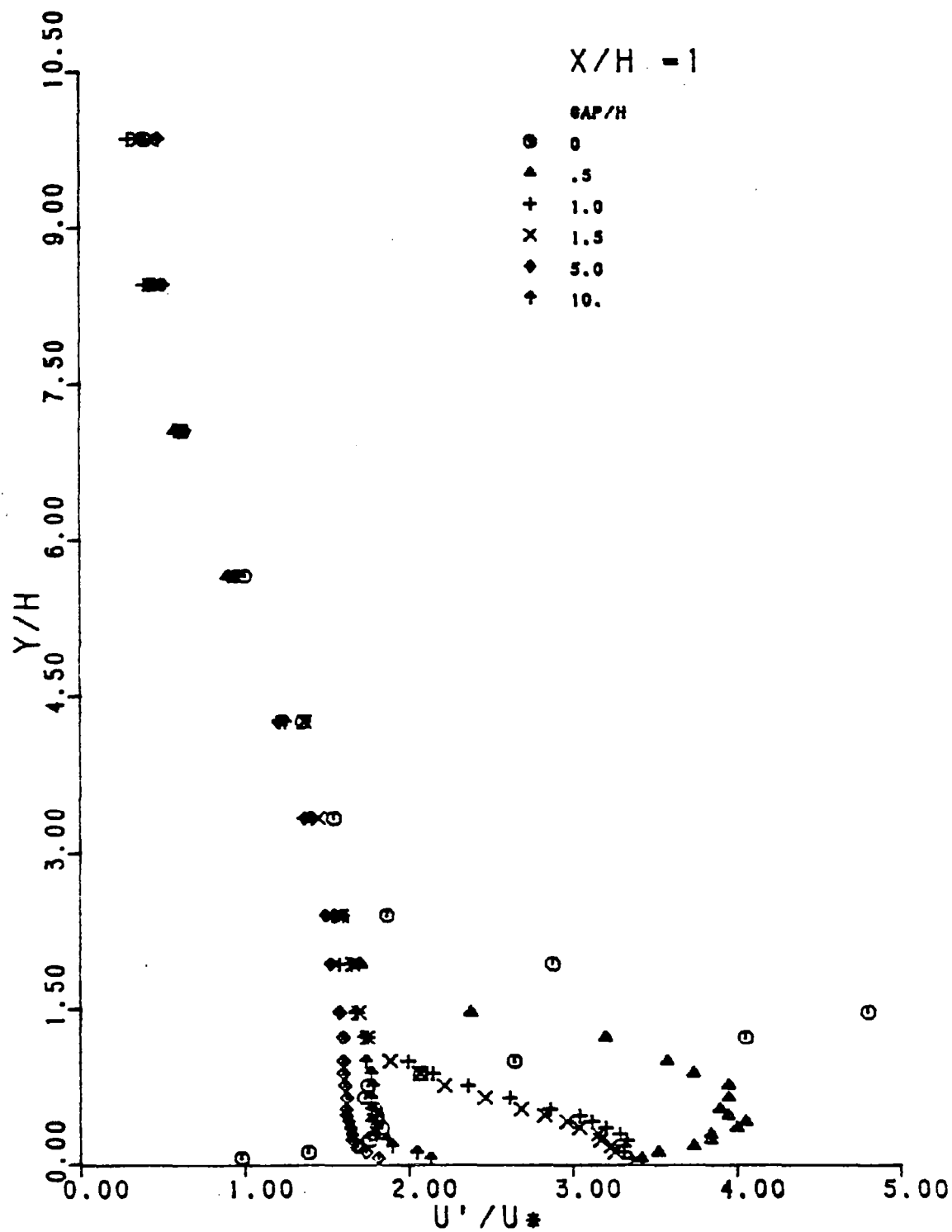
Fig. 24     Comparison of Longitudinal Turbulence Intensity,
x/H = 1.

37
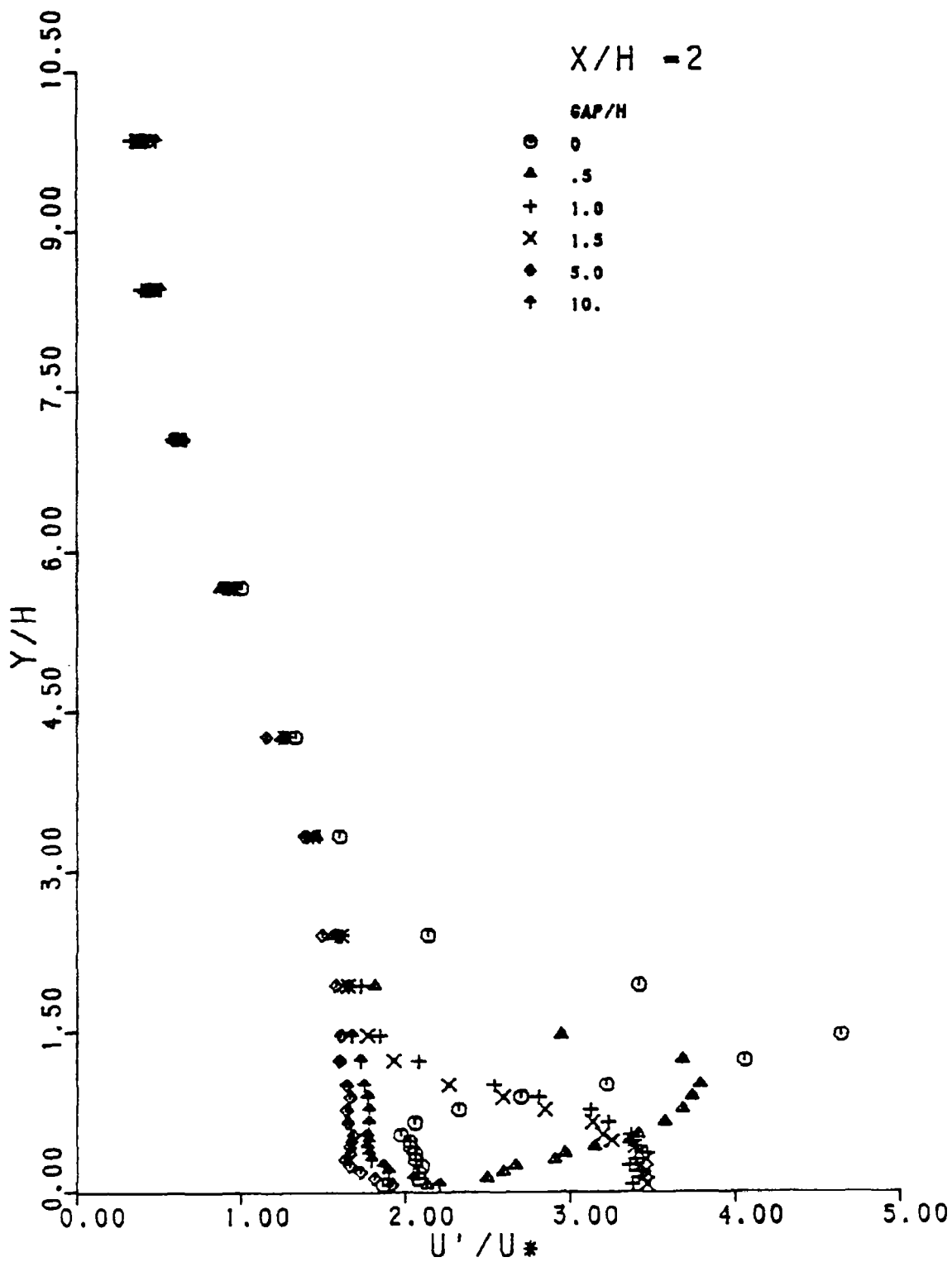
Fig. 25    Comparison of Longitudinal Turbulence Intensity,
x/H = 2.

38
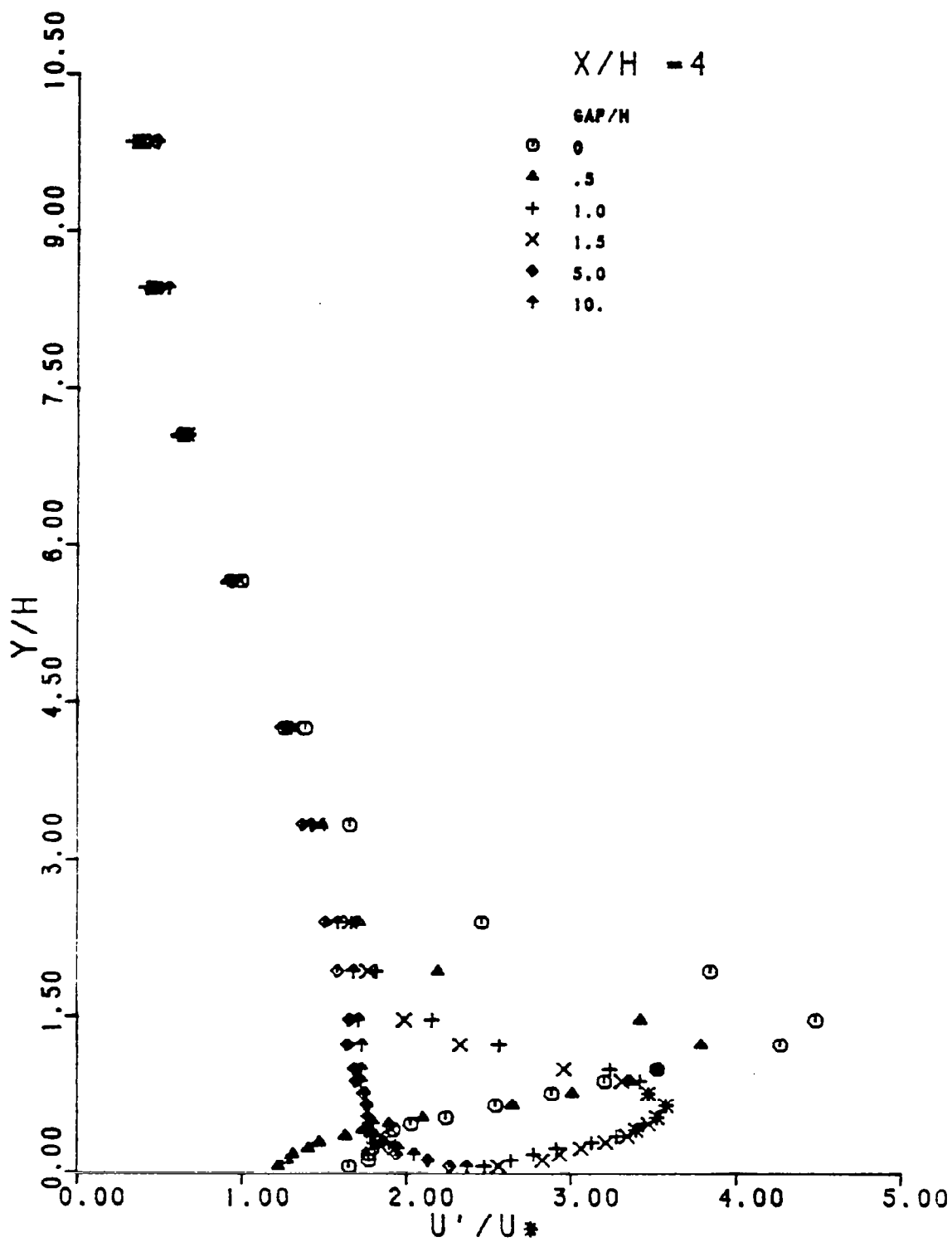
Fig. 26     Comparison of Longitudinal Turbulence Intensity,
            x/H = 4.
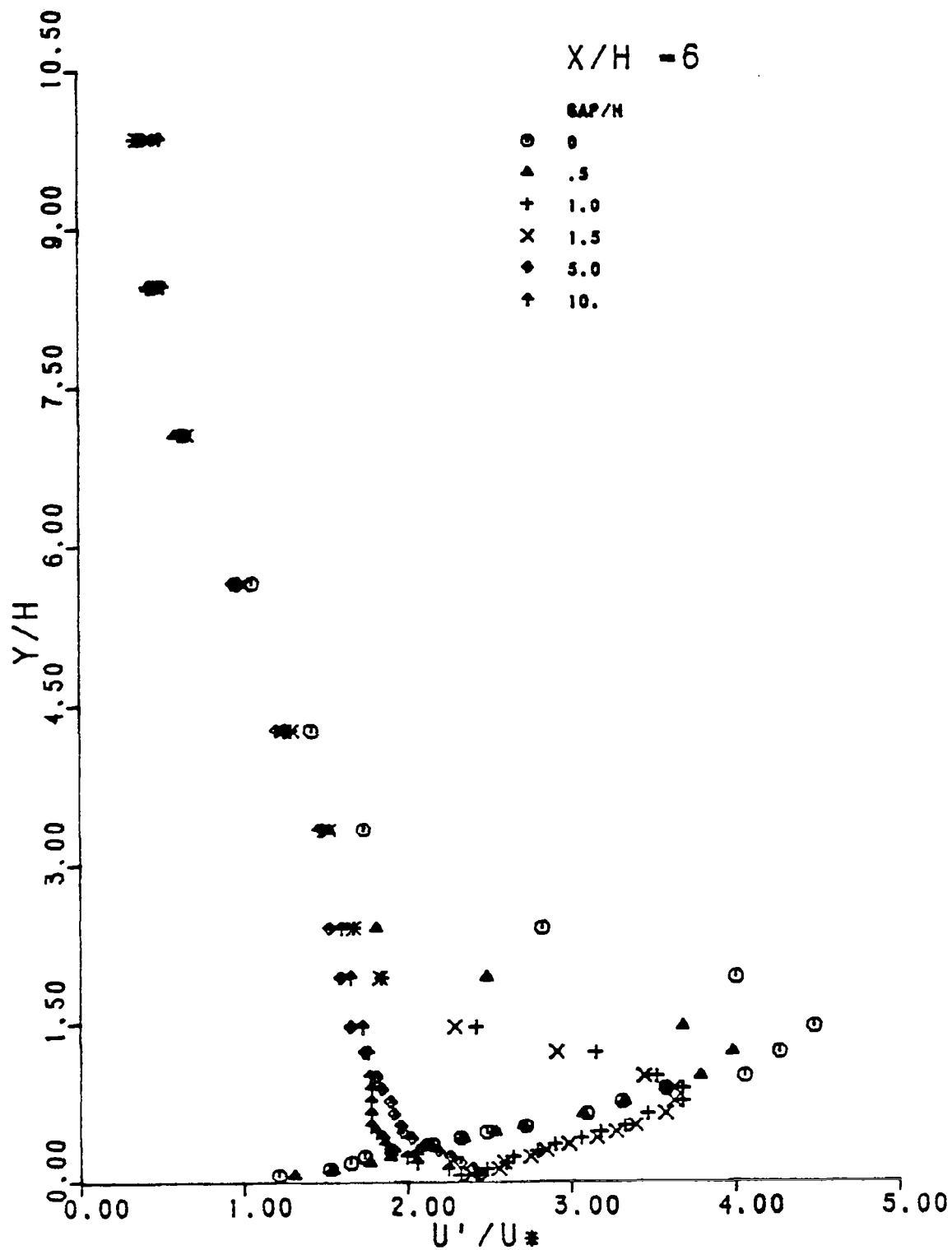
Fig. 27    Comparison of Longitudinal Turbulence Intensity,
x/H = 6.

40
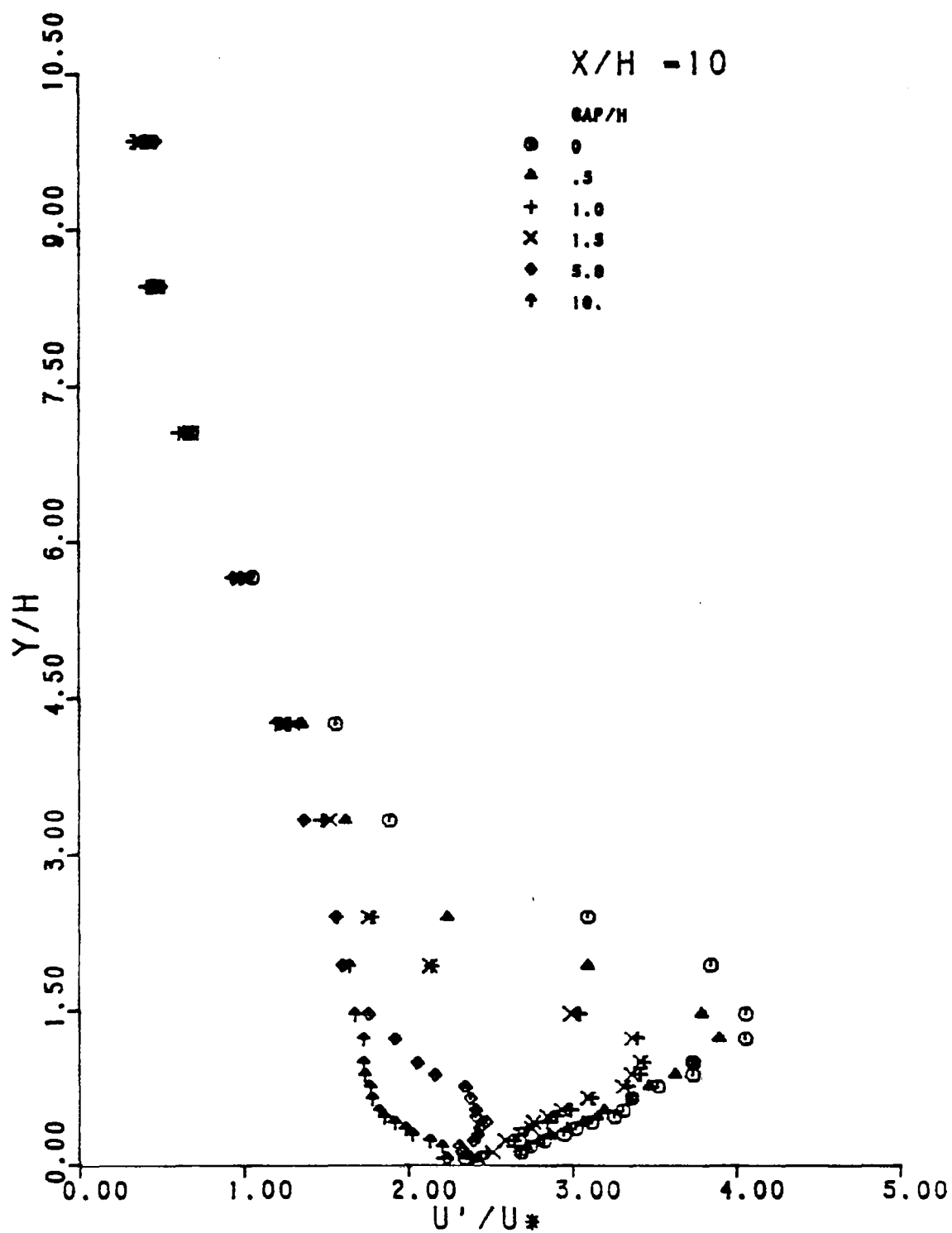
Fig. 28    Comparison of Longitudinal Turbulence Intensity.
x/H = 10.
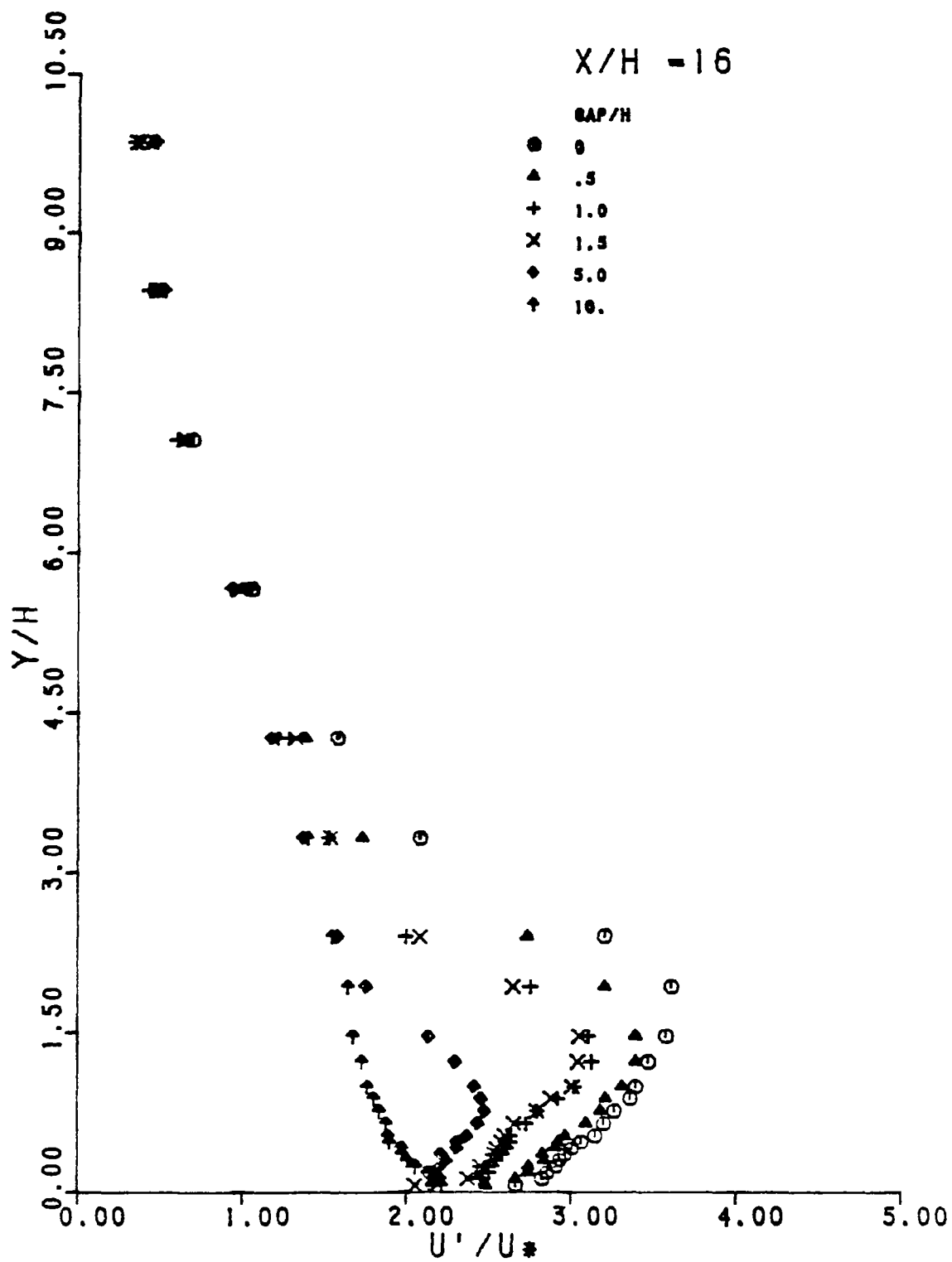
Fig. 29    Comparison of Longitudinal Turbulence Intensity,
x/H = 16.

42
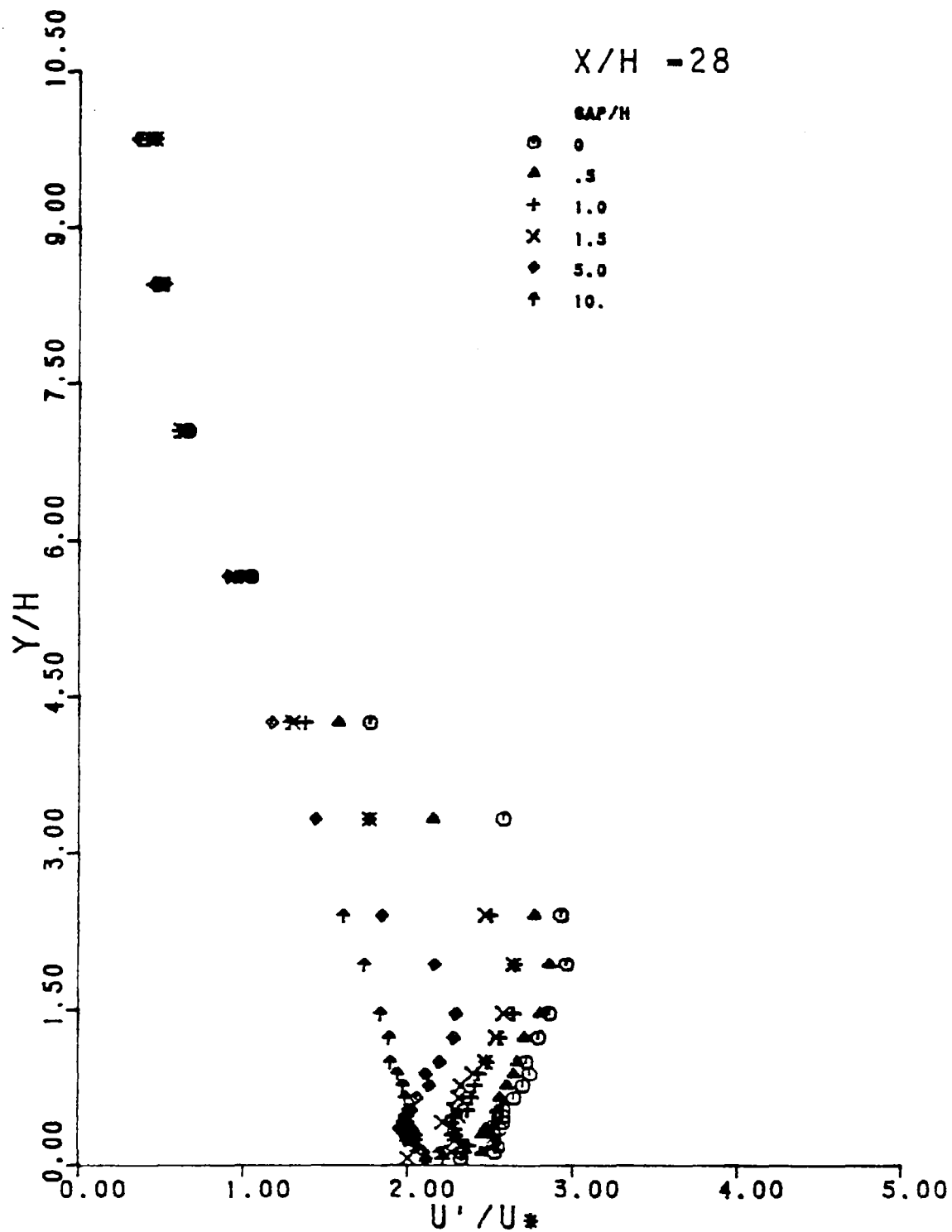
Fig. 30    Comparison of Longitudinal Turbulence Intensity, x/H = 28.

43
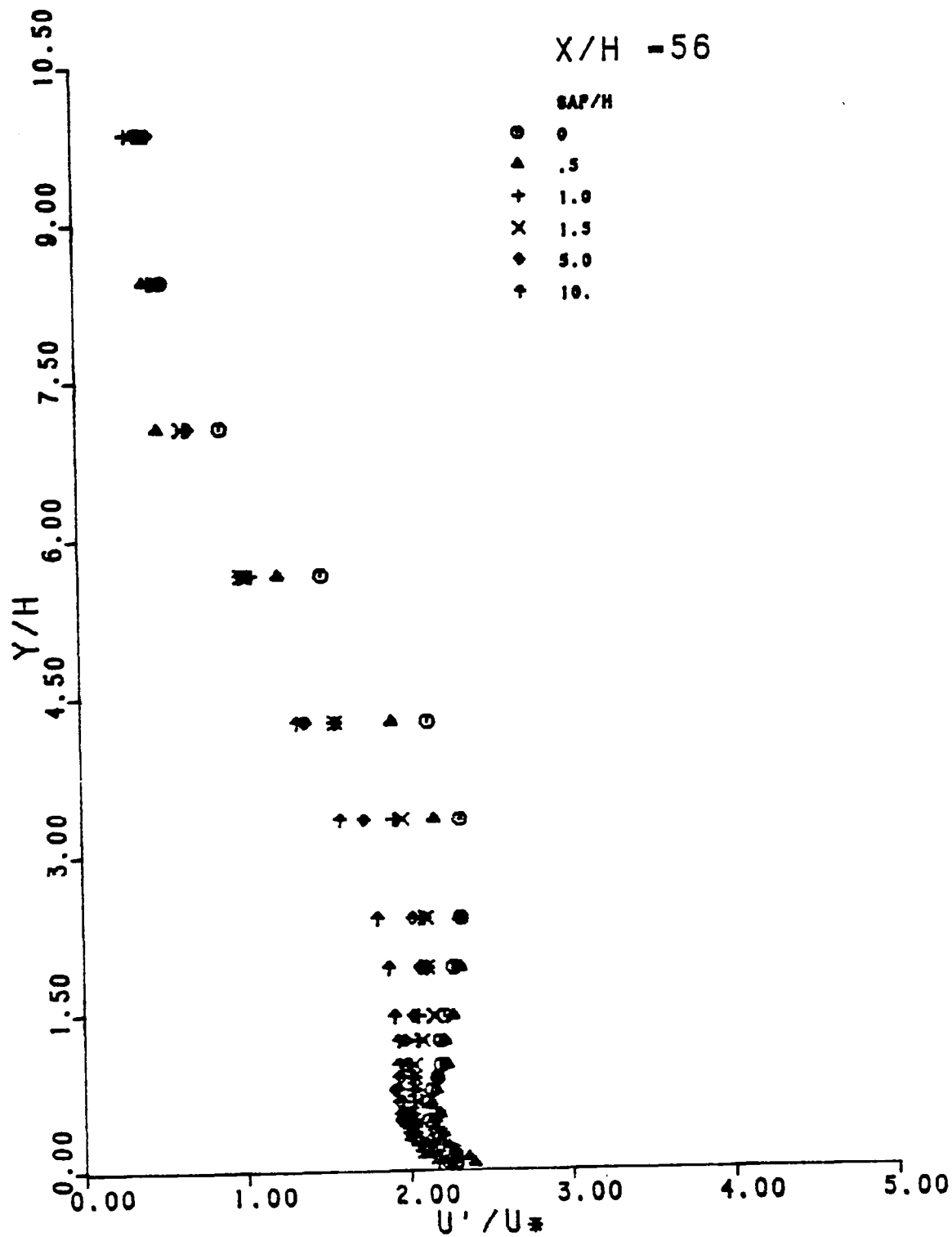
Fig. 31    Comparison of Longitudinal Turbulence Intensity,
x/H = 56.
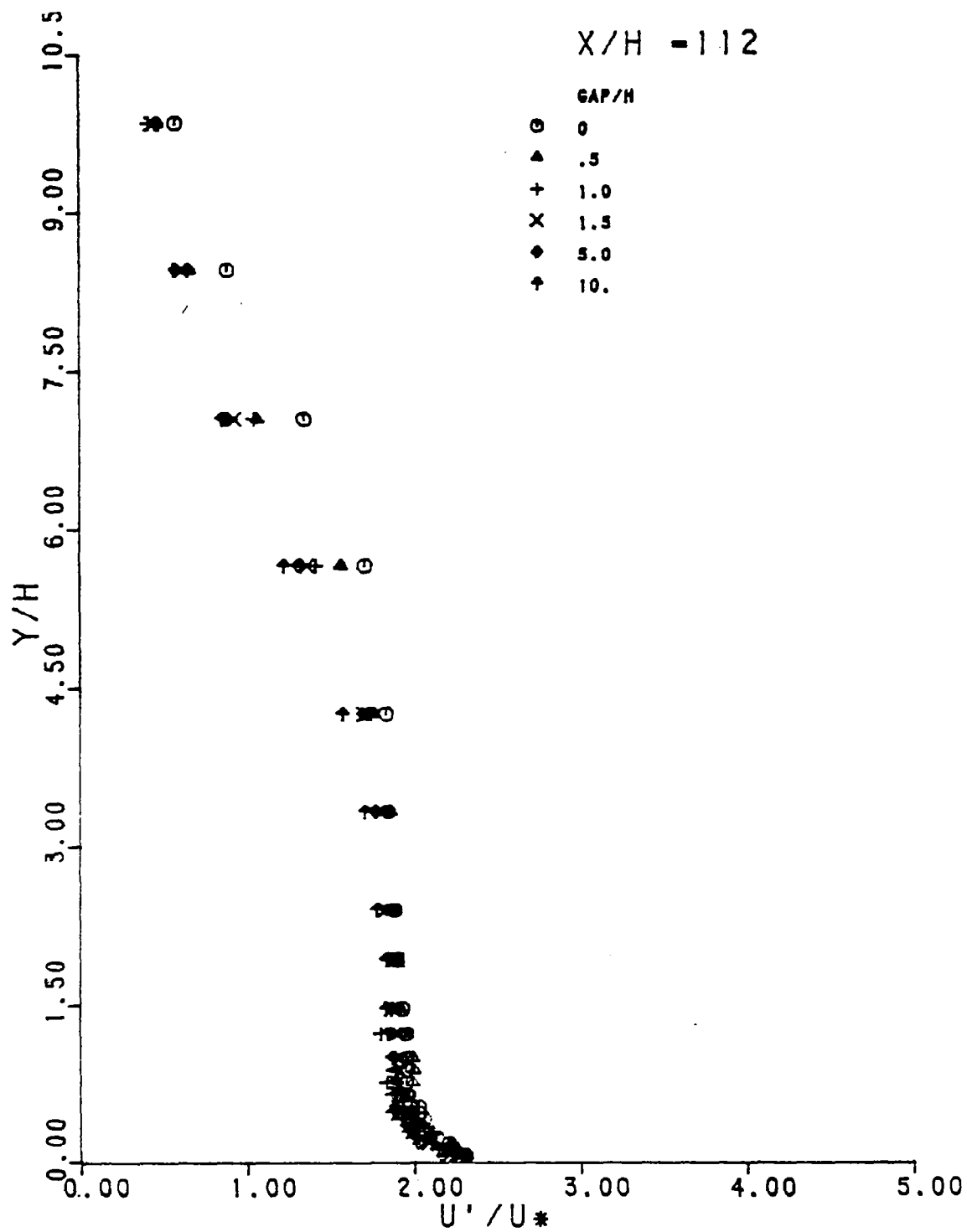
Fig. 32      Comparison of Longitudinal Turbulence Intensity,
x/H = 112.
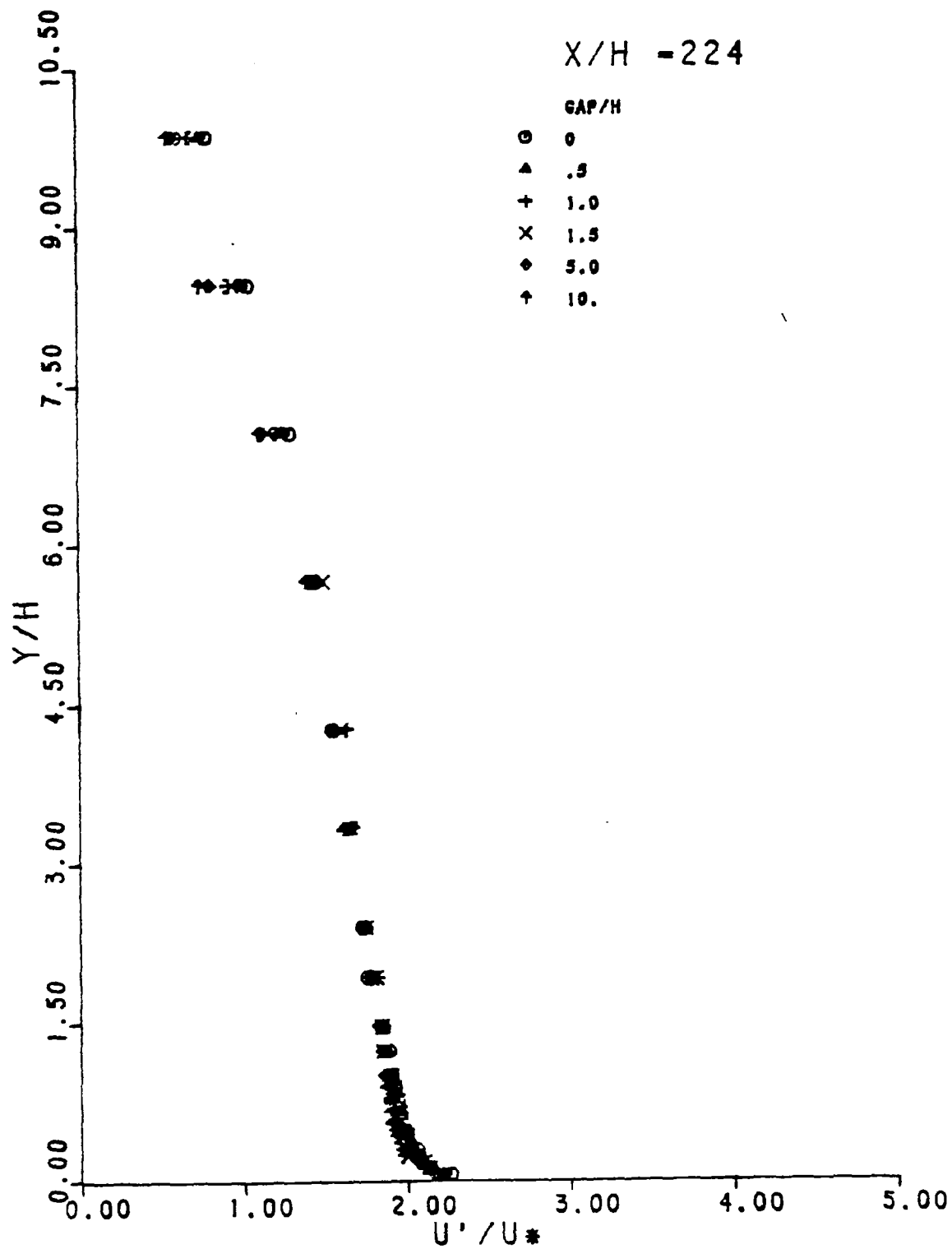
Fig. 33    Comparison of Longitudinal Turbulence Intensity,
x/H = 224.

# CHAPTER 4

## EFFECT OF SPACING

## LONGITUDINAL MEAN VELOCITY

As the smooth channel flow reaches a gap between elements, it is accelerated due to a "venturi-like" effect. This acceleration can be seen by comparing the smooth channel profile with the profiles at x/H=0 (rear of the element) for various gap sizes (Fig. 12). The flow begins to slow down just downstream from the gap as shown by Figs. 13-15. The point of maximum retardation of the flow for the various gap sizes is listed in Table 2.

When the mean velocity profile is plotted using a semi-logarithmic axis, "knee" points can be seen. The upper knee points as discussed by Siuru and Logan (1977) indicate the growth of the internal boundary layer after a change in roughness or other pertubation to the flow. These points are determined from the graphs and are depicted in Fig. 34. Siuru and Logan (1977) determined that the internal boundary layer thickness grows in proportion to $(x/H)^{\frac{1}{2}}$ with a change in roughness. As can be seen from Fig. 34 the no-gap case agrees qualitatively with their result, but the exponent is closer to 1/5. When a small gap exists (i.e., GAP/H = .5, 1.0, or 1.5), this same trend is found although at a different coefficient of proportionality. As the gap size increases, the "knee" points become

47

TABLE 2

Locations of Maxima and Minima

| GAP/H | X/H | | |
|-------|-----|-----|-----|
| | Maximum Retardation of Mean Velocity | Minimum $C_f$ | Maximum Longitudinal Turbulence Intensities |
| 0.5 | 4 | 4-6 | 6 |
| 1.0 | 4-6 | 4-6 | 6 |
| 1.5 | 6 | 4-6 | 6 |
| 5.0 | 16-28 | 21 | 16 |
| 10.0 | 56 | 224 | 56 (Y>H) |
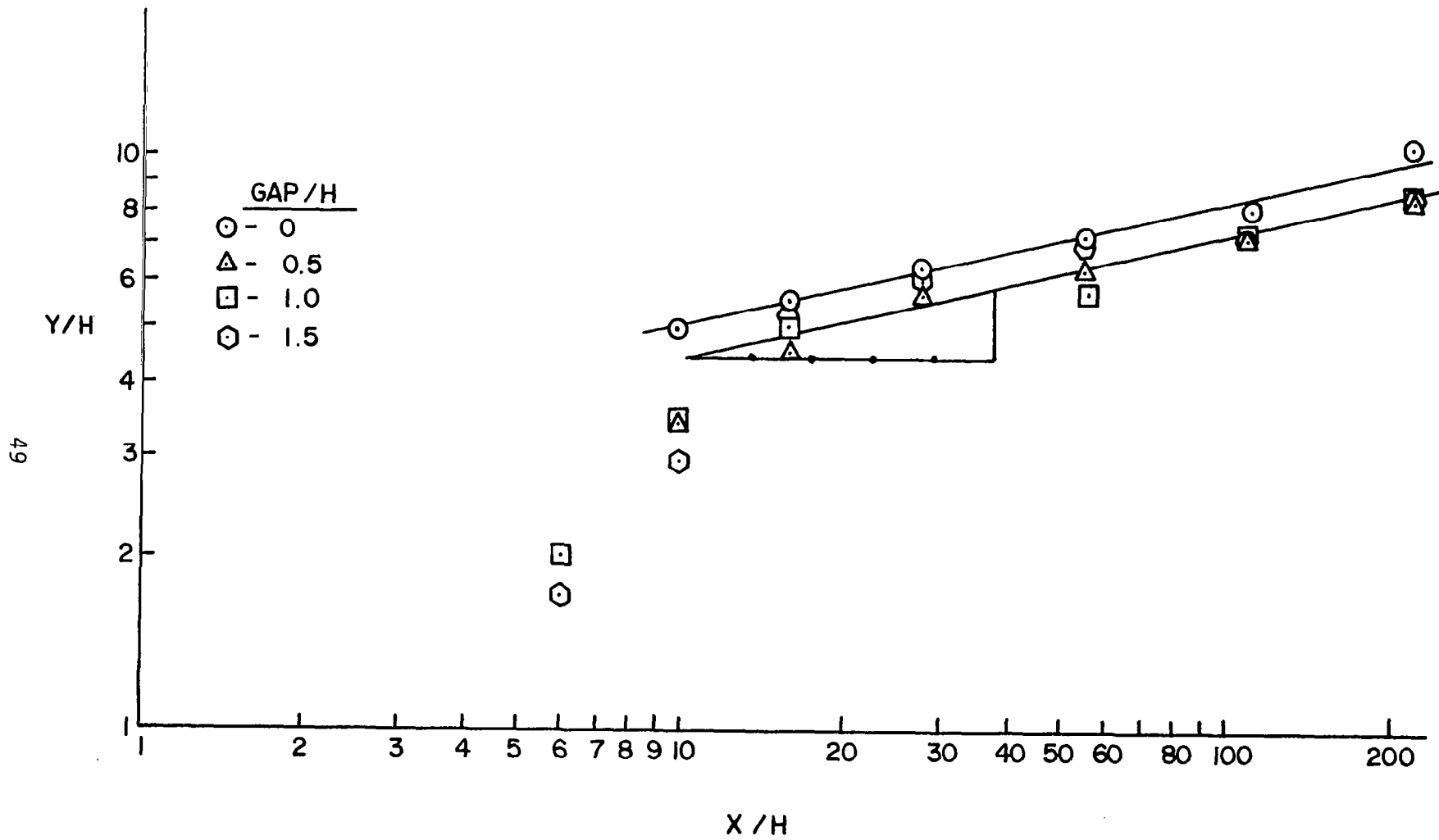
Fig. 34  Upper Knee Points for Different Gaps

49

less distinguishable. For the large gaps (GAP/H = 5.0 and 10.0), no correspondence was observed.

For the case x/H = 0, additional profiles were measured. These are at GAP/H = 2.0, 3.0, and 4.0, and were recorded in order to determine the gap at which the flow has the maximum acceleration. A venturi accelerates the flow in inverse proportion to the area of the nozzle exit. In this case, however, the fluid is able to flow over the obstacle rather than through the gap and less acceleration occurs in small gap sizes. As shown in Fig. 12, the gap size in which maximum acceleration occurs is between GAP/H = 1.5 and 2.0. It is also interesting to note that the profile of GAP/H = 10. resembles that of GAP/H = .5, and compared to the smooth channel profile, these flows are only slightly accelerated.

Figs. 13 through 22 compare the mean velocity profiles for various stations downstream. At x/H = 1 (Fig. 13), the profile GAP/H = .5 shows a slowing and begins to approach the profile of the no gap case. At this location, the profiles of GAP/H = 5 and 10 are not much different from the x/H = 0 case. The profiles at x/H = 2 and 4 (Figs. 14, 15) show a continuation of this trend. GAP/H = .5 has approximately modeled that of GAP/H = 0 by x/H = 4. The profiles at x/H = 6, 10 and 16 (Figs. 16 to 18) indicate a trend towards modeling by the GAP/H = .5, 1.0, and 1.5 profiles of the no-gap case. At x/H = 28 (Fig. 19), the GAP/H = 5.0 profile has also continued this trend, and by x/H = 56 (Fig. 20) the GAP/H = 10 profile has a similar characteristic. The profiles at x/H = 224 (Fig. 22) are nearly similar to that of smooth channel flow.

## SKIN FRICTION COEFFICIENT

The coefficient of floor friction, $C_f$, was calculated using the method described by Clauser (1954). Using the logarithmic law as a basis, straight lines are plotted on a chart of $U/U_1$ versus $\log_{10}(yU_1/\nu)$ for different values of $C_f$ according to the formula

$$U/U_1 = \sqrt{C_{f/2}}2.3/\kappa\log_{10}(yU_1/\nu)+\sqrt{C_{f/2}}(2.3/\kappa\log_{10}\sqrt{C_{f/2}}+A)$$

The constants $\kappa$ and $A$ are .41 and 5.0, respectively, as suggested by Coles and Hirst (1969). The data points for each mean velocity profile are then plotted on this graph. Data points in the logarithmic region correspond to the same slope as the "Clauser" lines, and thus the skin friction is determined. Due to the inaccuracies in determining the exact height of the probe above the floor, an error in origin on the "Clauser" graphs was noticed. This required a shift in some data points in order to determine the skin friction. This procedure is discussed by Perry et al. (1969).

Since the assumption was made that a logarithmic region exists, no skin friction coefficients can be determined with this method if the flow is separated from the surface. The point of reattachment, however, can be determined by extrapolating the line of best fit through the points downstream from reattachment in a graph of $C_f$ vs. $x/H$. This is shown in the GAP/H = 0 case in Fig. 35, and the reattachment point is estimated to be between 8-9 times the height of the obstacle downstream. This value agrees with that of Chang (1978) for a similar case. This figure also indicates the differences in the skin friction coefficient with the various gap sizes. The smaller gap sizes tend to resemble the no gap case but with slightly higher friction

51
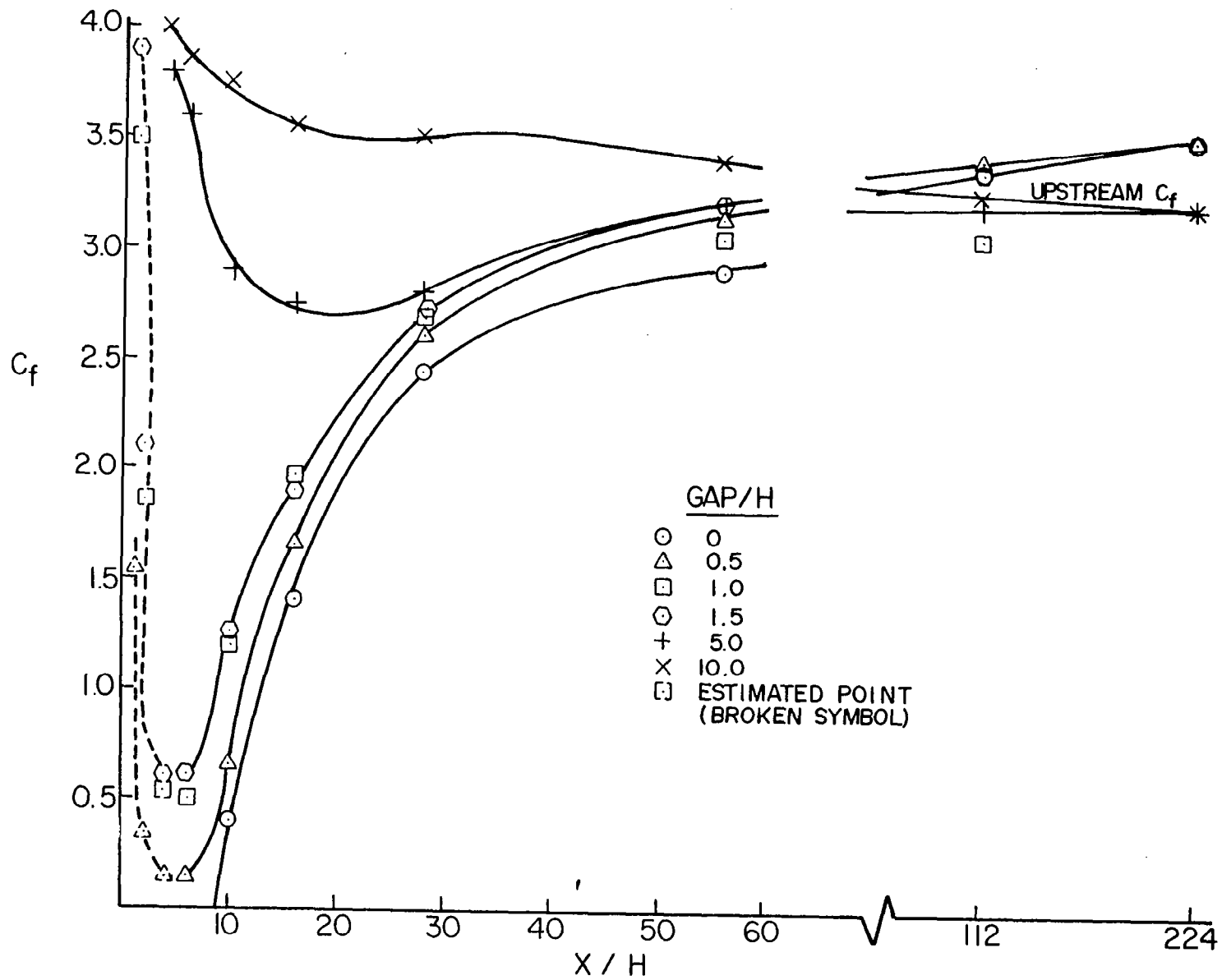
Fig. 35  Coefficient of Skin Friction for Different Gaps

52

coefficients. The estimated values (shown by the dashed lines) are found from the position of the profile on the Clauser plot, although a definite logarithmic portion could not be determined. These values indicate that there is no separation downstream along the centerline of the gap. The locations of the minimum $C_f$ for each gap is shown in Table 2, except for GAP/H = 10 where no depression was noted.

The values of the skin friction coefficient were compared with that of Mueller and Robertson (1962) and Petryk and Brundrett (1967). The graph presented in Mueller and Robertson (1962) of $C_f$ versus x/H agrees qualitatively with the no gap case, although their values of $C_f$ were higher and their reattachment point (x/H = 6.8) was earlier. From the small amount of data presented by Petryk and Brundrett (1967), the skin friction coefficient is generally lower than the present case, probably due to their highly smooth surface. In each of these studies, however, the $C_f$ value increased more rapidly and returned to equilibrium sooner than the no gap case. This phenomenon appears to depend on the height of the obstacle compared to the boundary layer thickness ($\delta$/H). It can be concluded that $C_f$ builds up and returns to equilibrium more slowly if the $\delta$/H is larger. From Fig. 35, it also should be noted that there is an apparent overshooting of the smooth channel value for the small gaps at x/H = 224 and an undershooting for the larger gaps. This same overshooting can be seen in the results of Bradshaw and Wong (1972).

Figure 35 shows the effect of the gaps on the attainment of an equilibrium value of $C_f$. If a very small perturbation were to interrupt this

flow, the $C_f$ value would soon return to the upstream value. As the perturbation becomes larger, more deviation from the upstream value will be noted and the $C_f$ would return more slowly. In this case, the $C_f$ curve for GAP/H = 10 deviates very little from the smooth channel $C_f$. As the gap size is decreased, however, more deviation is noted and return to the upstream flow is slower.

## EQUILIBRIUM SHAPE FACTOR

The equilibrium shape factor, G, was calculated according to the formula

$$G = \int_0^\delta \left(\frac{U_1-U}{U*}\right)^2 d\,(y/\Delta)$$

where

$$\Delta = \int_0^\delta \left(\frac{U_1-U}{U*}\right) dy$$

This parameter was first developed by Clauser (1954) and he concluded that G = 6.8 represented the equilibrium boundary layer flow condition for zero pressure gradient (Clauser, 1956). Other values have also been reported. In the present study, the upstream value of G was calculated to be 6.41. Using the smooth channel case as the reference value, it can be seen by Fig. 36 that the GAP/H = 0, .5 and 1.5 have "undershot" this value at x/H = 224. It appears that the GAP/H = 5 and 10 cases have slightly overshot the reference value. This same undershooting effect was noticed by Bradshaw and Wong (1972), who concluded that G does not return monotonically to its equilibrium value. They also found that a minimum value of G will occur at

$$x/H = 100\,\sqrt{\delta/H}$$

54
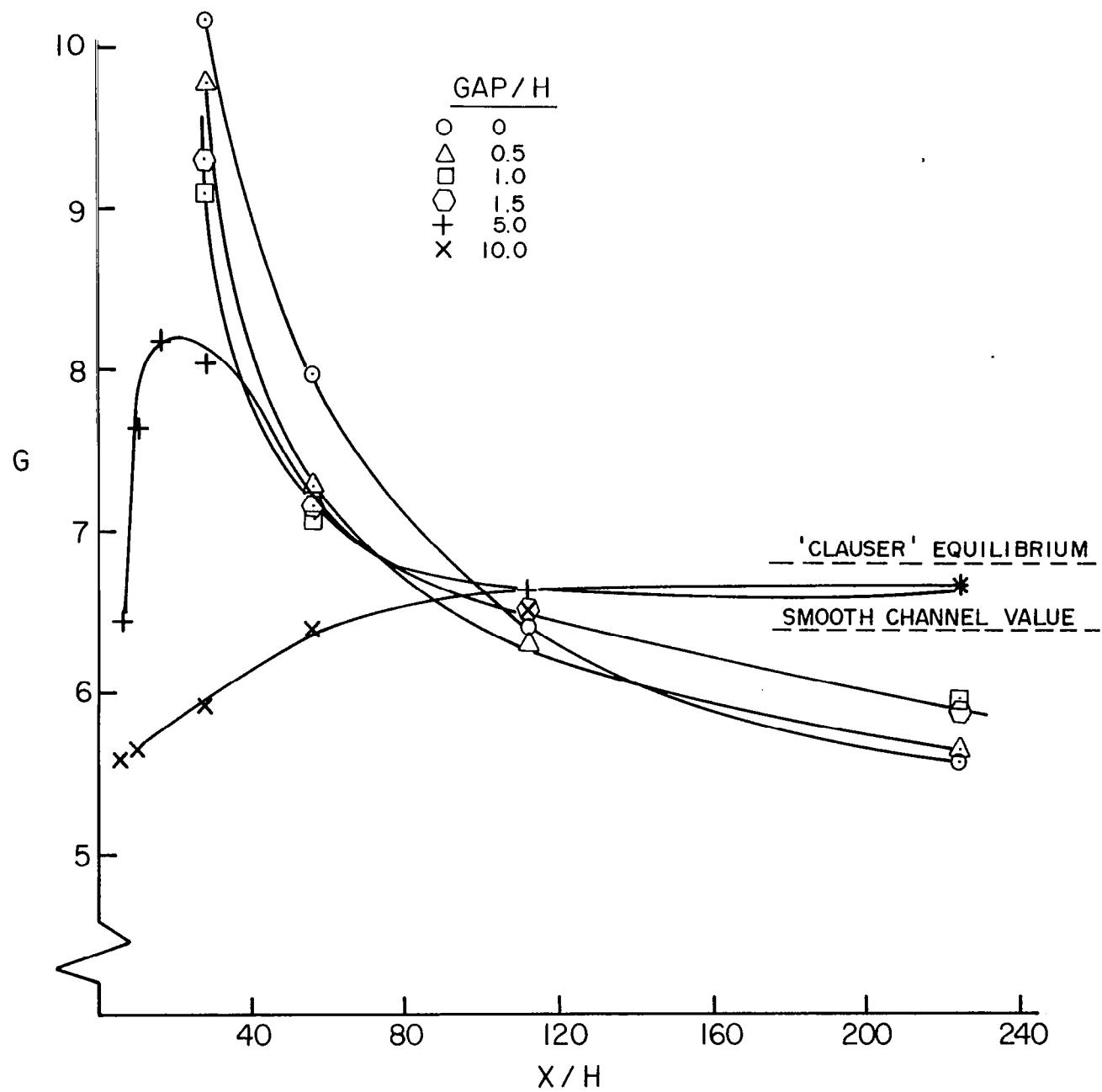
Fig. 36    Clauser Shape Factor for Various Gaps

For the present no-gap case, this minimum point would occur at x/H = 316.

The effect of the gap is to moderate the flow disturbance. For small or no gap the value of G rises abruptly and then undershoots its final value. For larger gaps the disturbance is small and the return to equilibrium swift; in fact, for GAP/H = 5 and 10 no minimum is observed. The effect of an increase in size on $C_f$ and G appears to be equivalent to a reduction of H, or an increase of $\delta$/H, in the two-dimensional case (no-gap case).

## LONGITUDINAL TURBULENCE INTENSITY

As shown by Figs. 23 through 33, the point of maximum turbulence intensity occurs in the wake just above the element for the no-gap case. As the downstream distance increases, the point of maximum turbulence intensity gradually moves up, away from the floor, and the maximum turbulence intensity decreases.

As can be seen in Fig. 23, except for the smallest gap, the longitudinal turbulence intensity has been reduced by the gap. The acceleration in the gap, as seen by Fig. 23, has reduced the velocity gradient $\partial U/\partial y$ and consequently the rate of turbulence production is reduced. As opposed to other gap sizes, the GAP/H = 0.5 case shows a turbulence increase with two points of maximum intensity. This increase is thought to be the result of two effects. The first is the high velocity gradients created at the ends of the elements due to the accelerated flow in the gap and the separation zone immediately behind the roughness element. This produces high turbulence intensity where these two effects meet. The second is the "horse-shoe" vortices which are assumed to exist in front of the elements and move downstream

through the gap. Such vortices could move the high intensity turbulence
created by the velocity gradient near the model ends to the centerline
of the gap where it is measured. The turbulence would have a maximum intensity
at a lower height due to the motion of these vortices. The effects of the
horse-shoe or trailing vortices, however, cannot be directly seen in any
other profile downstream, and the presence of the vortices has not yet been
confirmed by flow visualization.

As the distance downstream increases, the turbulence intensities also
increase until a maximum occurs. The locations of the maxima are shown in
Table 2. The height and value of the maximum intensity are lower than the
no-gap case, and the fact that maxima are produced further downstream from
wider gaps implies a spanwise propagation of the distortion effect from the
wake flows directly behind the obstacle. The significance of secondary
currents associated with the vortices has not been assessed to date.

After the point of maximum turbulence intensity, the shape of the tur-
bulence intensity profiles suggest that each gap has begun to model that
of the no gap case. This phenomena can be seen in Fig. 26 for GAP/H = .5,
Figs. 27 and 28 for GAP/H = 1.0 and 1.5, and Fig. 29 for GAP/H = 5.0. At
$x/H = 224$ (Fig. 33), no difference can be seen in the turbulence intensities,
and they nearly resemble that of the smooth channel case.

CHAPTER 5

CONCLUSIONS

The following conclusions are drawn from velocity and turbulence measurements made in a wind tunnel for wakes formed downstream of gaps between two equal sized building models for GAP/H of 0.5, 1.0, 1.5, 5.0 and 10.0.

1.  The upstream flow is accelerated through the gap between rough-ness elements.  The maximum acceleration occurs with a gap size of 1.5 to 2.0 times the element height.

2.  Immediately downstream from the gap, the flow begins to slow down with the distance to the point of maximum retardation a function of the gap size.

3.  After the point of maximum retardation, the mean velocity profiles become similar to the no gap case.

4.  The coefficient of skin friction indicates that there no separation region is formed along the centerline downstream from each gap.

5.  The effect of an increase in gap size is to hasten the attainment of the equilibrium value of $C_f$.

6.  The equilibrium shape factor results indicate that an increase in gap size is equivalent to increasing $\delta/H$ for a single two-dimensional obstacle.

7.  The flow downstream from a large gap (5.0, 10.0) has nearly reached equilibrium by $x/H = 224$.

8. The longitudinal turbulence intensity begins to model the turbulence intensity of the case with no-gap at a certain point downstream. The location of this point is a function of gap size.

9. After the modeling takes place, the maximum turbulence intensity will be less and at a lower height for the flow with a gap, than for the flow without a gap, compared at the same $x/H$.

10. The effects of horseshoe vortices may explain the unusual profile at $x/H = 0$ for the GAP/H = .5, but their effects were not obvious elsewhere.

11. A gap size of 10 times the element height has only a slight effect on the flow as observed on the centerline at downstream stations.

# REFERENCES

Arie, M. and Rouse, H. (1956), Experiments on two-dimensional flow over a normal wall. J. Fluid Mech. 1, 129-141.

Benedict, Robert P. (1977), Fundamentals of temperature, pressure, and flow measurements. John Wiley and Sons, New York, 2nd Ed., 343-350.

Bradshaw, P. and Wong, F. Y. F. (1972), The reattachment and relaxation of a turbulent shear layer. J. Fluid Mech. 52, Part 1, 113-125.

Castro, I. P. (1971), Wake characteristics of two-dimensional perforated plates normal to an airstream. J. Fluid Mech. 46, Part 3, 599-609.

Castro, I. P. and Robins, A. G. (1977), The flow around a surface-mounted cube in uniform and turbulent streams. J. Fluid Mech. 79, No. 2, 307-335.

Chang, J. E. (1978), Perturbation of turbulent pipe flow by roughness elements. M.S. Thesis, Arizona State University.

Clauser, Francis H. (1954), Turbulent boundary layers in adverse pressure gradients. J. Aeronautical Sci., Vol. 21, 91-108.

Clauser, Francis H. (1956), The turbulent boundary layer. Advances in Applied Mechanics, Vol. IV, 1-51.

Coles, D. E. and Hirst, E. A. (1969), Computation of turbulent boundary layers - 1968. AFOSR-IFP-Stanford Conference Vol. II, Stanford University, Calif.

Counihan, J., Hunt, J.C.R. and Jackson, P.S. (1974) Wakes behind two-dimensional surface obstacles in turbulent boundary layers. J. Fluid Mech., Vol. 64, 529-563.

Fichtl, George H., Camp, Dennis W. and Frost, Walter (1977), Sources of low-level wind shear around airports. J. Aircraft, Vol. 14, No. 1, 5-14.

Frost, W., and A.M. Shahabi (1977), A field study over a simulated block building. NASA CR-2804, NASA/Marshall Space Flight Center, AL.

Frost, W., Fichtl, G., Connell, J.R. and Hutto, M.L. (1977), Mean horizontal wind profiles measured in the atmospheric boundary layer about a simulated block building. Boundary-Layer Meteorology, Vol. 11, 135-145.

Good, M.C. and Joubert, P.N. (1968), The form drag of two-dimensional bluff plates immersed in turbulent boundary layers. J. Fluid Mech. 31, 547-582.

Klebanoff, P.S. and Diehl, Z.W. (1951), Some features of artificially thickened fully developed turbulent boundary layers with zero pressure gradient. Natl. Advisory Com. for Aeronautics, Tech. Note 2475.

Kline, S.J. and McKlintock, F.A. (1953), Describing uncertainties in single-sample experiments. Mech. Eng. 3-8.

Logan, E. and D. W. Camp (1978) Preliminary comparison of model and proto-type wakes. AIAA Paper No. 78-254.

Logan, E. and Chang, J. (1980) Wake characteristics of buildings in disturbed boundary layers. NASA CR-3284, NASA/Marshall Space Flight Center, AL.

Mueller, Thomas J. and Robertson, M.R. (1962), A study of the mean motion and turbulence downstream of a roughness element. Proc. First Southeastern Conf. on Theoretical and Applied Mechanics, 326-340.

Mueller, T J., Korst, H. H. and Chow, W. L. (1964), On the separation, reattachment and redevelopment of incompressible turbulent shear flow. Trans. ASME, J. Basic Engr. 221.

Oka, S. and Kostic, Z. (1971), Flowfield past a single roughness element in channel of rectangular cross-section. Heat and Mass Transfer in Boundary Layers, Vol. 1, Pergamon Press Ltd., New York, 425-435.

Oka, S. and Kostic, Z. (1972), Influence of wall proximity on hot-wire velocity measurements. DISA Information No. 13, 29-33.

Perry, A.E., Schofield, W.H. and Joubert, P.N. (1969), Rough wall turbulent boundary layers, Part 2. J. Fluid Mech., 37, 383-413.

Petryk, S. and Brundrett, E. (1967), Recovery of a turbulent boundary layer disturbed by a single roughness element. Res. Rept. No. 4, Dept. of Mech. Eng., University of Waterloo.

Phataraphruk, P. and Logan, Jr., E. (1978), Response of a turbulent pipe flow to a single roughness element. Proc. Ninth Southeastern Conf. on Theoretical and Applied Mechanics, 139-149.

Plate, Erich J. (1967), Diffusion from a ground level line source into the disturbed boundary layer for downstream from a fence. Int. J. Heat Mass Transfer, Vol. 10, 181-194.

Plate, E.J. (1971), Aerodynamic Characteristics of Atmospheric Boundary Layers, Springfield, National Technical Information Service.

Sami, Sedat and Liu, Weirjuan Henry (1975), Confined shear layer approaching a stagnation point. Proc. 14th Midwestern Mech. Conf. Developments in Mechanics, Vol. 8, 497-516.

Sháran, V. Kr. (1975), On characteristics of flow around building models with a view to simulate the minimum fraction of the natural boundary layer. Intl. J. Mech. Sci. Vol. 17, 557-563.

Siuru, Jr., W.D. and Logan, Jr., E. (1977), Response of a turbulent pipe flow to a change in roughness. Transactions of the ASME, J. Fluids Eng., 548-555.

Sundaram, T.R., Ludwig, G.R. and Skinner, G.J. (1972), Modeling of the turbulence structure of the atmospheric surface layer. AIAA J. Vol. 10, 743-750.

Thinh, Nguyen Van (1969), On some measurements made by means of a hot wire in a turbulent flow near a wall. DISA Information No. 7, 13-18.

Tielman, H.W. and Sandborn, V.A. (1965), A three-dimensional single roughness element in a turbulent boundary layer. Defense Documentation Center, Defense Supply Agency, No. AD 623-902.

Wieghardt, K. (1953), Erhöhung des turbulenten Reibungswiderstandes durch Oberflachenstörungen. Forschungshefte fur Schiffstechnik, Vol. 1, 65-81.

Woo, H.G.C., Peterka, J.A. and Cermak, J.E. (1977), Wind-tunnel measurements in the wakes of structures. NASA CR-2806, NASA/Marshall Space Flight Center, AL. 35812.

APPENDIX

UNCERTAINTY ANALYSIS

An uncertainty analysis was performed on this experiment in order to describe a possible value of the error. The estimates of the uncertainty in each of the variables are shown in Table 3. These uncertainty intervals are based on the odds 20 to 1. The estimates of the uncertainty in each of the variables are based on the following factors where applicable.

slight differences in the level of the wind tunnel

floor due to alignment or the inherent distortions

of the wood.

small differences in the precise location of the elevation

of the probe above the floor.

random errors in the reading of instruments due to

fluctuating signals.

time dependent drift of the hot wire anemometer.

errors in mean velocities due to the hot wire measuring the

resultant velocities of the longitudinal and lateral components,

rather than the longitudinal components.

The effect of the uncertainty in each variable on the uncertainty of the derived results was based upon the work of Kline and McClintock (1953). The uncertainty of the derived results can be expressed as:

$$\frac{W_r}{R_e} = \left[ \left( \frac{\partial R}{\partial V_1} \frac{W_1}{R_e} \right)^2 + \left( \frac{\partial R}{\partial V_2} \frac{W_2}{R_e} \right)^2 + \ldots + \left( \frac{\partial R}{\partial V_N} \frac{W_N}{R_e} \right)^2 \right]^{\frac{1}{2}}$$

where R is a linear function of N independent variables, $W_i$ is the uncertainty interval for the independent variable $V_i$, and $R_e$ is the result of the linear function R. The estimates of uncertainty for the derived data by using the above equation are tabulated in Table 4.

# TABLE 3

## Estimates of Uncertainty in Measured Data

| Measured Quantity | Percent Uncertainty Interval (20 to 1) | Remarks |
|---|---|---|
| Side walls of wind tunnel | 0.142 | Physical dimension |
| Slope of wind tunnel roof | 0.798 | Physical dimension |
| Height/width of roughness elements (H) | 1.51 | Physical dimension |
| Longitudinal pressure gradient ($\Delta P$) | 0.275 | Fixed error for constant flow rate |
| Mean velocity measured by hot wire (U) | 6.2 | Random error-electronic instrument |
| Longitudinal turbulence intensity (U') | 4.8 | Random error-electronic instrument |
| Friction factor (CF) | 2.50 | Random error-from graphical analysis |
| Laboratory temperature | 0.668 | Random error-surrounding conditions |
| Laboratory pressure | 0.175 | Random error-surrounding conditions |
| Centerline mean velocity (U1) | 0.227 | Random error-electronic instrument |

TABLE 4

Estimates of Uncertainty in Derived Data

| Parameter | Percent Uncertainty Interval (20 to 1) | Remarks |
|---|---|---|
| 1. Reynolds number $(\frac{U_1 H}{\nu})$ | 1.53 | |
| 2. Longitudinal velocity $(U/U_1)$ | 8.0 $(y<H)$, 0.9 $(y\simeq\delta)$ | Greatest values- close to floor and within separation zone |
| 3. Longitudinal turbulence $(U'/U^*)$ | 6.8 $(y<H)$, 5.9 $(y\simeq\delta)$ | Greatest value- close to floor and within separation zone |
| 4. Friction velocity $(U^*)$ | 2.79 | |

| 1. REPORT NO.<br>NASA CR-3337 | 2. GOVERNMENT ACCESSION NO. | 3. RECIPIENT'S CATALOG NO. |
|---|---|---|
| 4. TITLE AND SUBTITLE<br><br>Effect of Lateral Spacing on Wake Characteristics of Buildings | | 5. REPORT DATE<br>November 1980 |
| | | 6. PERFORMING ORGANIZATION CODE |
| 7. AUTHOR(S)<br>Earl Logan, Jr., and David S. Barber | | 8. PERFORMING ORGANIZATION REPORT # |
| 9. PERFORMING ORGANIZATION NAME AND ADDRESS<br><br>College of Engineering and Applied Sciences<br>Arizona State University<br>Tempe, Arizona 85281 | | 10. WORK UNIT NO.<br>M-306 |
| | | 11. CONTRACT OR GRANT NO.<br>NAS8-32357 |
| | | 13. TYPE OF REPORT & PERIOD COVERED |
| 12. SPONSORING AGENCY NAME AND ADDRESS<br><br>National Aeronautics and Space Administration<br>Washington, D.C. 20546 | | Contractor Report |
| | | 14. SPONSORING AGENCY CODE |

15. SUPPLEMENTARY NOTES

NASA Marshall Technical Monitor: M. B. Alexander
Final Report

16. ABSTRACT

Measurements relevant to the effect of buildings on the low-level atmospheric boundary layer are presented. A wind tunnel experiment was undertaken to determine the nature of the flow downstream from a gap between two transversely aligned, equal-sized models of rectangular cross section. These building models were immersed in an equilibrium turbulent boundary layer which was developed on a smooth floor in a zero longitudinal pressure gradient. Measurements of the longitudinal mean velocity and longitudinal turbulence intensity were made using a hot wire anemometer in the plane of symmetry of the wake downstream of the gap. The size of the gap was varied from the case which resembled a single continuous element (no gap) to that which resembled smooth channel flow (very large gap). Quantitative results are presented which show that the three-dimensional wake has no recirculation zone and that widening the gap produces a far wake much like the wake behind a two-dimensional obstacle of smaller height.

| 17. KEY WORDS<br><br>Wind Profile<br>Wake Turbulence | 18. DISTRIBUTION STATEMENT<br><br>Unclassified – Unlimited<br><br>STAR Category 47 | |
|---|---|---|
| 19. SECURITY CLASSIF. (of this report)<br><br>Unclassified | 20. SECURITY CLASSIF. (of this page)<br><br>Unclassified | 21. NO. OF PAGES<br>74 | 22. PRICE<br>A04 |